scientific reports

Check for updates

OPEN

Variable scale operational path planning for land levelling based on the improved ant colony optimization algorithm

Wenming Chen[1], Jiaxin Yang[1], Shaocen Zhang[1], Xinhua Wei[1,2]✉, Chengliang Liu[3], Xinying Zhou[1], Lei Sun[1], Fei Wang[1] & Anzhe Wang[1]

To address the challenges associated with traditional traversal-based land leveling, which often suffered from a lack of coordination and planning, resulting in low operational efficiency and the management of large data volumes in contemporary path planning, this study proposed a variable-scale improved ant colony optimization algorithm specifically designed for land leveling path planning. The research introduced the IACO (Improved Ant Colony Optimization) algorithm for large-scale inter-region soil balance path planning, alongside the FIA*ACO (Fusion of the Improved A* Ant Colony Optimization) algorithm for small-scale, fine-grained full-field leveling path planning. Based on the analysis of actual field experiments, the inter-regional levelling operation resulted in a 47.5% reduction in the maximum elevation difference of the path, a 26.3% increase in the distribution of the 5 cm elevation difference, and a 53.7% improvement in flatness. In contrast, the refined levelling operation achieved a 62.9% reduction in the maximum elevation difference, a 52.0% increase in the distribution of the 5 cm elevation difference, and a 78.4% enhancement in flatness. These findings suggested that regional path planning could effectively enhance the area of fields meeting leveling standards, whereas fine-gridded path planning further optimized the leveling effect. This confirmed the efficacy of the scale-variable improved ant colony optimization algorithm in land leveling path planning.

Keywords Land leveling, Path planning, IACO, FIA*ACO, Variable-scale optimization

Land leveling is a crucial step in modern agriculture, directly impacting irrigation efficiency, crop yields, and land use effectiveness[1–3]. Currently, leveling operations are typically conducted using parallel or spiral line traversals, or are randomly selected by the operator based on visual inspection, often without coordination or planning[4–7]. Most operational paths derived from digital maps of farmland are subjectively chosen, lacking comprehensive optimization[8–10]. This results in frequent occurrences of 'full-load dragging' and 'empty running,' which lead to low efficiency and high fuel consumption. Consequently, there is an urgent need for the development of path planning methods for leveling operations to reduce fuel consumption and enhance efficiency.

In recent years, automatic navigation technology has increasingly been applied to land leveling operations. Path planning for these leveling operations is a critical component of automatic navigation in farmland leveling. The leveling machine adjusts its travel state by measuring the lateral and heading errors relative to the planned path. Utilizing global navigation satellite system (GNSS), the difference between the elevation of the operation point and the reference height is measured, enabling the hydraulic cylinders to control the vertical movement of the leveling blade for excavation or filling tasks[11,12]. Liu et al. utilized the shortest empty and full load times of the loader as the optimal evaluation criterion. They clustered farmland grids to facilitate global leveling path planning by employing designed excavation and filling methods in conjunction with local search strategies. However, this evaluation focused solely on minimizing the shortest times for empty and full loads, neglecting soil movement efficiency, which resulted in longer path planning times[13]. Kang et al. proposed a global path planning method that effectively reduced ineffective operation time to some extent. Nevertheless, their approach only addressed minimizing the number of ineffective empty/full load operations, steering actions, and repetitive traversals, while failing to consider the comprehensive load rate of the leveling blade, which led to longer

[1]School of Agricultural Engineering, Jiangsu University, Zhenjiang, China. [2]Key Laboratory for Theory and Technology of Intelligent Agricultural Machinery and Equipment of Jiangsu University, Jiangsu University, Zhenjiang, China. [3]School of Mechanical Engineering, Shanghai Jiao Tong University, Shanghai, China. ✉email: 15190419393@163.com

path distances[14]. Jin et al. introduced a three-dimensional (3D) path planning method for farmland leveling navigation based on an improved ant colony algorithm, aiming for efficient soil transport and the shortest path. However, this method was limited to planning one path at a time, resulting in lower operational efficiency[15]. Ojima et al. demonstrated that dynamic programming could be effectively applied to land leveling, allowing for dynamic path adjustments based on the leveling blade load; however, the computational complexity increased significantly with the number of nodes[16]. Jeon et al. employed a genetic algorithm to identify the optimal inner trajectory for paddy fields by minimizing head-turning distances and traversing the entire field. However, this method was susceptible to local optima[17]. Jing et al. introduced a constraint on the minimum turning radius of the leveling machine and proposed an enhanced MOEA/D-FMACO algorithm to determine the optimal autonomous leveling path. This approach was grounded in multi-objective optimization that considered travel distance, steering angle, and earthwork volume. Nonetheless, they overlooked the leveling blade load as an optimization objective, which led to an increase in repetitive operations[18]. The research status of land leveling path planning both domestically and internationally was shown in Table 1.

To address the challenges posed by large data volumes, inadequate consideration of the leveling blade load, and the limitations of single-path planning in the previously discussed leveling operation path planning, this paper investigated a scale-variable improved ant colony optimization algorithm for continuous path planning. We proposed an enhanced ant colony optimization algorithm specifically designed for large-scale inter-regional earthwork balance path planning. Additionally, we developed a hybrid approach that integrated improved A* and ant colony optimization algorithms for small-scale fine-grading operation path planning across the entire farmland. This research provided a comprehensive technical framework for the global optimization of leveling operation paths.

Materials and methods

Establishment of farmland terrain model and regional division

This study employed the grid-based method for modeling the farmland terrain. Initially, terrain data for the farmland was captured using unmanned aerial vehicles (UAVs) mapping[19], followed by processing the information into grids. Each elevation point across the terrain was organized within the grid. The grid value corresponded to the earthwork volume information within each grid cell. The volume of earthwork needing excavation or filling in each grid cell was computed to serve as the foundation for path planning. It was presumed that the earthwork volume in excavation grids would be positive, whereas in filling grids, it would be negative. For example, the gridded terrain data for a piece of farmland was illustrated in Fig. 1. To streamline path planning, the grid size was initially defined as 1 m but should be scaled up threefold for actual computations.

The region-growing utilized the principle of similarity to combine pixels that had common attributes, resulting in the formation of larger regions with similar characteristics. The key steps included the following.

Step 1: Identify position (x, y), which served as the initial core seed point, where $f(x, y)$ was the corresponding grid value, and $\tilde{f}(x, y)$ referred to the grid values of the four neighboring grids around (x, y) (top, bottom, left, and right). Equation (1) presented the primary condition for the region growing process. The first growth process of the region was illustrated in Fig. 2.

$$\left|\tilde{f}(x, y) - f(x, y)\right| \leq T \tag{1}$$

Authors	Contribution	Shortage	Experience
Liu et al.	Taking the shortest shovel empty or full load time as the optimal evaluation benchmark, clustering farmland grids, and according to the designed shovel dig-high-fill-low method and local search strategy to get the global planning of levelling paths	Only the shortest empty and full load time of the grading shovel was used as an evaluation index, without considering the efficiency of earth volume transport, and the path planning time was long	Path planning for flatland operations is a multi-objective optimization problem
Kang et al.	A global path planning method was proposed, which could plan effective paths and reduce the ineffective operation time to some extent	The least ineffective operation status of empty and full load, the least steering operation and repeated travelling were taken as evaluation indexes, the combined load ratio of the levelling shovel was not taken into account, and the distance of the planned path was long	Path planning for flatland operations is a multi-objective optimization problem
Jin et al.	A three-dimensional path planning method based on improved ant colony algorithm for farmland levelling navigation was proposed for the purpose of reasonable earth transport and unloading with the shortest path in levelling operation	Only able to plan paths in a single pass, with low operational efficiency	Dynamic continuous planning of paths is required for efficient levelling
Ojima et al.	It was demonstrated that the dynamic programming algorithm could be applied to the land levelling problem and dynamically adjusted the planning path according to the load of the levelling shovel	The arithmetic power increased abruptly with more nodes	Fields need to be zoned first to reduce planning time
Jeon et al.	Genetic algorithm was used to determine the optimal sequence of internal trajectories in a paddy field by minimizing the turning distance at the head of the field and traversing the entire field	It was easy to fall into local optimal solution, a flaw of the genetic algorithm itself	The selection of path planning algorithm needs to consider high global search capability and robustness
Jing et al.	A tri-objective (travel distance, steering angle, earthwork) problem was modelled and an improved (model decomposition and further mutation ant colony) multi-objective evolutionary algorithm was used to optimize the grading path	Failure to include grading shovel load characteristics as one of the optimization objectives to increase the number of repetitive round trips	Path planning for flatland operations is a multi-objective optimization problem

Table 1. Current status of domestic and international research in path planning for land leveling path planning.

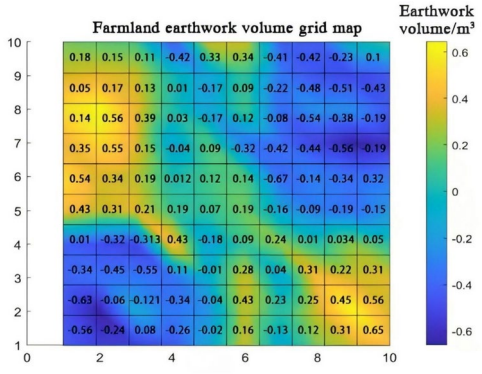

Fig. 1. Rasterization of farmland terrain information.

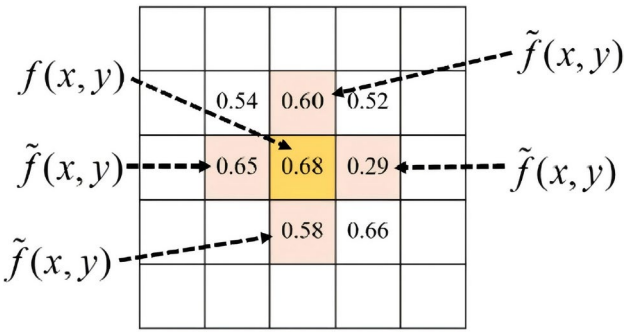

Fig. 2. First growth process of the region.

In the equation, T denoted the threshold for region growing.

Step 2: Upon completing the initial region growing process, the core seed point was updated to the mean value H_{ave} of the expanded seed point set $\mathcal{S}$, as detailed in Eq. (2).

$$H_{ave} = \frac{1}{n}\sum_{Si=1}^{n} f_{Si}\,(x,y) \tag{2}$$

In the equation, n denoted the total number of grids grown within set $\mathcal{S}$, and $f_{Si}\,(x,y)$ referred to the earthwork volume of the i-th grid in set S, m^3.

Step 3: The newly incorporated growth points in set $\mathcal{S}$ would have their adjacent grid points (top, bottom, left, and right) designated as candidate growth points. Grid points that satisfied the growth criteria outlined in Eq. (3) would be merged into the target region.

$$\left|\tilde{f}(x,y) - H_{ave}\right| \leq T \tag{3}$$

Step 4: Repeat steps 2 and 3 until the region growth was complete.

Inter-regional operation path planning based on the IACO

Establishment of objective function for inter-regional operation path planning

Assume that $V_i = (V_1, V_2, \ldots, V_m)$ represented the scraper's work volume at the i-th node along the path, where excavation was positive and filling was negative. The current path passed through m nodes. The ratio of the total work performed along the entire path to the distance of the current path, denoted as $F_{transport}$, was presented in Eq. (4).

$$F_{transport} = \frac{\sum_{i=1}^{m}|V_i|}{L_{sum}} \tag{4}$$

In the equation, L_{sum} denoted the distance between the starting grid and the ending grid, m.

In this study, empty load travel was defined as the distance between the final operational grid in the high-terrain region and the first operational grid upon entering the low-terrain region, and the distance from the last

operational grid in the low-terrain region to the first operational grid in the high-terrain region. The empty load travel ratio was calculated as outlined in Eq. (5).

$$F_{empty} = \frac{L_{empty}}{L_{sum}} \tag{5}$$

In the equation, L_{empty} denoted the empty load travel distance along the path, m.

The objective function for inter-regional operation path planning was presented in Eq. (6). A lower objective function value indicated greater operational efficiency for the inter-regional path.

$$F_{region} = \omega_1 \cdot \frac{1}{F_{transport}} + \omega_2 \cdot F_{empty} \tag{6}$$

In the equation, ω_1 and ω_2 were weight coefficients, $\omega_1 \in (0,1)$, $\omega_2 \in (0,1)$, and $\omega_1 + \omega_2 = 1$.

Design of the IACO algorithm

When the levelling scraper was operating in a high-terrain region, the optimal neighborhood search algorithm could identify the excavation operation path in the high-terrain and the filling operation path in the low-terrain. By considering the earthwork volume along the operational search path between the high and low-terrain regions as heuristic information[20], the transition probability $p_{ij}^{z}(t)_{HighToLow}$, was presented in Eq. (7).

$$p_{ij}^{z}(t)_{HighToLow} = \begin{cases} \frac{[\tau_{ij}(t)]^{\alpha}[\eta_{ij}(t)\mu_{ij}(t)]^{\beta}}{\sum_{s \in allowed_z} [\tau_{is}(t)]^{\alpha}[\eta_{is}(t)\mu_{is}(t)]^{\beta}} & If\ j \in allowed_z \\ 0 & Other \end{cases} \tag{7}$$

In the equation, $allowed_z$ denoted the set of next regions for ant z to move towards; α referred the pheromone weighting factor; β denoted the heuristic function weighting factor; μ_{ij} referred the total amount of soil to be moved along the search path from region i to region j, as shown in Eq. (8).

$$\mu_{ij} = \sum_{M_h=1}^{M_H} |V_{m_h}| + \sum_{n_l=1}^{N_L} |V_{n_l}| \tag{8}$$

In the equation, M_H denoted the number of grids along the operational search path in the high-terrain region; V_{m_h} referred the amount of soil to be moved when passing through the m_h-th grid in the high-terrain region, m^3; N_L denoted the number of grids along the operational search path in the low-terrain region; V_{n_l} referred the amount of soil to be moved when passing through the n_l-th grid in the low-terrain region, m^3.

When the levelling scraper was in a low-terrain region, the ratio of the earthwork volume to be moved in the target high-terrain region to the scraper's maximum load was also considered as heuristic information[21]. Thus, the transition probability $p_{ij}^{z}(t)_{LowToHigh}$, was provided in Eq. (9).

$$p_{ij}^{z}(t)_{LowToHigh} = \begin{cases} \frac{[\tau_{ij}(t)]^{\alpha}\left[\eta_{ij}(t)\cdot\frac{V_j^r}{V_{\max}}\right]^{\beta}}{\sum_{s \in allowed_z} [\tau_{is}(t)]^{\alpha}\left[\eta_{is}(t)\cdot\frac{V_s^r}{V_{\max}}\right]^{\beta}} & If\ j \in allowed_z \\ 0 & Other \end{cases} \tag{9}$$

In the equation, V_j^r denoted the amount of earthwork to be moved in the next target high-terrain region, m^3.

In the ant colony optimization (ACO) algorithm, the weight factor of the heuristic function remained fixed and did not adapt based on historical optimal search path information during subsequent iterations. This limitation frequently caused the algorithm to become trapped in a local optimum. To address this issue, the optimization objective function values from both previous and current iterations, as well as the overall optimal search path up to the current iteration, were employed to adaptively modify the weight factor of the heuristic function. The method for this adaptive adjustment was outlined in Eq. (10).

$$\beta = \beta + \beta . \ln \frac{F_{region}(k-1)}{F_{region}(k)} \cdot \frac{F_{region}(k-1)}{F_{region}(best_k)} . e^{\frac{k}{k_{max}}} / Q_1 \tag{10}$$

In the equation, $F_{region}(best_k)$ denoted the optimization objective function value of the ant colony's optimal search path up to the k-th iteration; $F_{region}(k)$ referred the optimization objective function value of the ant colony's optimal search path in the k-th iteration; $F_{region}(k-1)$ denoted the optimization objective function value of the ant colony's optimal search path in the $(k-1)$-th iteration; $k_{\max}$ referred the total number of iterations; Q_1 was a constant, set to 2 in this paper.

The pheromone evaporation factor ρ influenced the pheromone update process in the ant colony algorithm[22]. To address this, a pheromone evaporation factor adjustment rule was introduced to adaptively modify the pheromone concentration along the paths, as presented in Eq. (11).

$$\rho(t+1) = \begin{cases} \rho_a \cdot \rho(t) & N_{best_{F_{region}}} \geq 5 \\ \rho_{\min} & \rho(t+1) < \rho_{\min} \end{cases} \tag{11}$$

In the equation, ρ_a denoted the pheromone evaporation factor weighting coefficient; $\rho(t)$ referred the pheromone evaporation factor at time t; $\rho_{\min}$ denoted the minimum pheromone evaporation factor; $N_{best_{F_{region}}}$ referred the consecutive iterations of the current optimal search path in the ant colony.

The pheromone increment $\Delta\tau_{ij}^{z}(t)'$ of the z-th ant after moving from region i to region j at time t was improved as shown in Eq. (12).

$$\Delta\tau_{ij}^{z}(t)' = \begin{cases} \frac{Q}{F_{region}} & From\ region\ i\ to\ region\ j \\ 0 & Others \end{cases} \tag{12}$$

In the equation, Q denoted the pheromone intensity coefficient, set to 10 in this paper; F_{region} referred the optimization objective function value of the optimal search path for the z-th ant up to the current iteration.

After the improvement, the pheromone concentration on the search path at time $(t+1)$ was updated according to Eq. (13).

$$\tau_{ij}'(t+1) = (1-\rho)\tau_{ij}(t)' + \sum_{z=1}^{Z_{ant}} \Delta\tau_{ij}^{z}(t)' \tag{13}$$

In the equation, $\tau_{ij}(t)'$ denoted the pheromone concentration on the path from the current region i to the next region j; Z_{ant} referred the total number of ants traveling from region i to region j.

To avoid premature convergence and prevent the ant colony from maturing too early, upper and lower bounds were imposed on the pheromone levels, as outlined in Eq. (14).

$$\tau_{ij}(t)' \begin{cases} \tau_{\max} & \tau_{ij}(t)' \geq \tau_{\max} \\ \tau_{\min} & \tau_{ij}(t)' \leq \tau_{\min} \\ \tau_{ij}(t)' & \tau_{\min} < \tau_{ij}(t)' < \tau_{\max} \end{cases} \tag{14}$$

In the equation, $\tau_{\max}$ denoted the upper limit of the pheromone, and $\tau_{\min}$ referred the lower limit of the pheromone.

The flowchart of inter-region earthwork balance operation path planning was shown in Fig. 3.

Full-field precision operation path planning based on the FIA*ACO

Establishment of objective function for full-field precision operation path planning

Assuming there were U nodes along this path, $V_{\mathcal{U}}$ denoted the earthwork volume managed by the grader at the $\mathcal{U}$-th node. The efficiency of earthwork transportation was provided in Eq. (15).

$$F_{Allregion} = \frac{\sum_{u=1}^{U} |V_u|}{L_{StartToEnd}} \tag{15}$$

In the equation, $L_{StartToEnd}$ denoted the distance of the path from the start grid to the end grid, m.

The sum of the grader blade load variation rates, V_p, was presented in Eq. (16).

$$V_p = \sum_{u=1}^{U} \frac{|V_u|}{V_{\max}} \tag{16}$$

In the equation, $V_{\max}$ denoted the maximum load of the grader blade, m^3.

The calculation rules for the steering factor $angle_i$, were as follows:

Suppose that in a planned operation path, the three adjacent grid nodes were r_{i-1}, r_i, and r_{i+1}, with corresponding coordinates (x_{i-1}, y_{i-1}), (x_i, y_i), and (x_{i+1}, y_{i+1}). Let vector $\vec{v}_1 = (x_i - x_{i-1}, y_i - y_{i-1})$ and $\vec{v}_2 = (x_{i+1} - x_i, y_{i+1} - y_i)$. The angle θ_i formed by the path of these three adjacent nodes could be expressed by Eq. (17).

$$\theta_i = \arccos\left(\frac{\vec{v}_1 \cdot \vec{v}_2}{\vec{v}_1 \cdot \vec{v}_2}\right) \tag{17}$$

The steering factor was assigned different values depending on the angles of the path, as outlined in Eq. (18).

$$angle_i = \begin{cases} 1 & 90^\circ < |\theta_i| < 180^\circ \\ 2 & 45^\circ < |\theta_i| \leq 90^\circ \\ 3 & |\theta_i| \leq 45^\circ \end{cases} \tag{18}$$

The steering objective function F_θ was defined as the sum of the steering factors $angle_i$ for all adjacent triplets of nodes along the path, as presented in Eq. (19). A lower function value corresponded to larger turning angle on the path, indicating smoother steering.

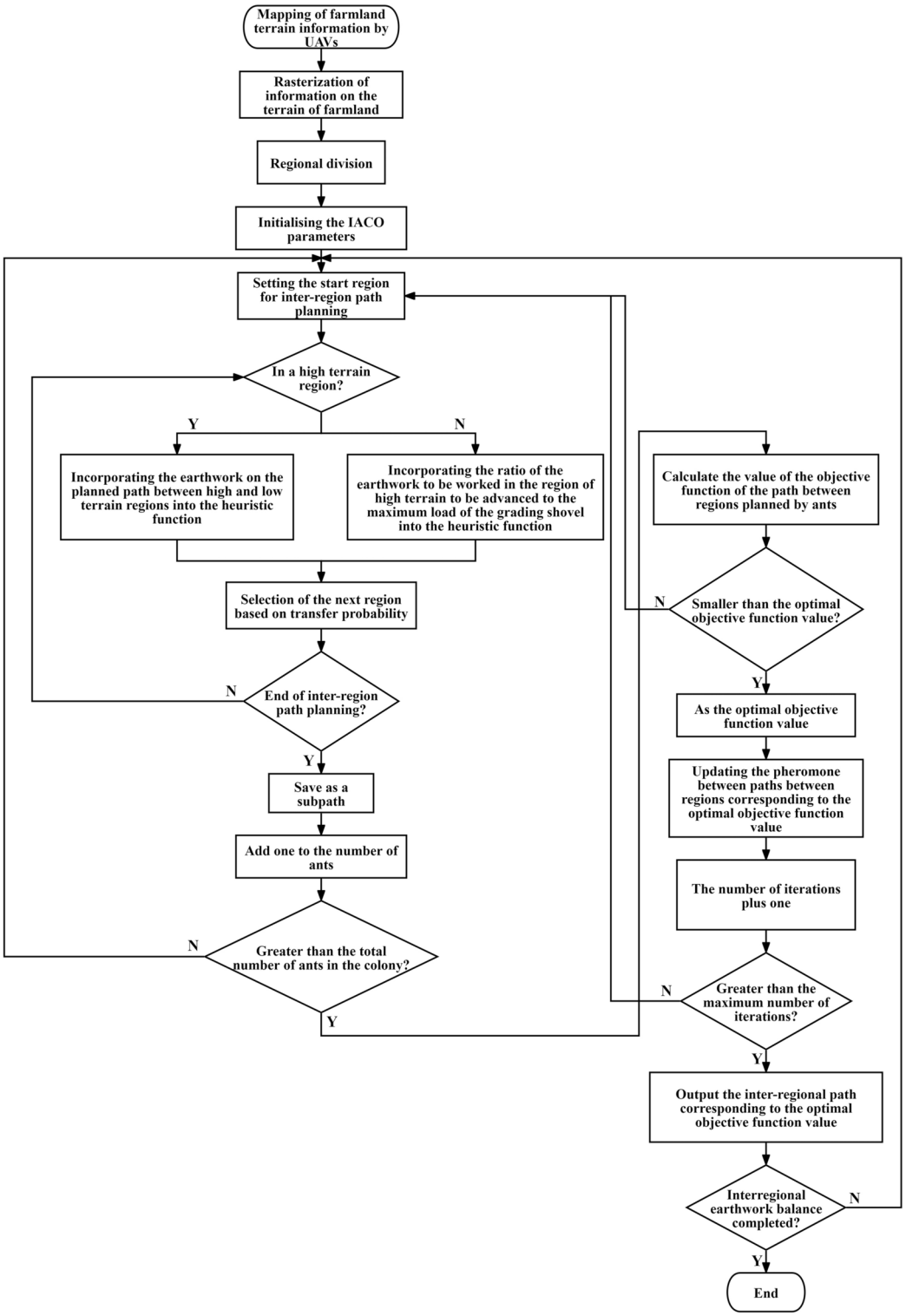

Fig. 3. Flowchart of inter-region earthwork balance operation path planning.

$$F_\theta = \sum_{i=2}^{U-1} angle_i \tag{19}$$

In the equation, U denoted the number of nodes on this path.

Thus, the objective function for the full-field precision operation path planning was formulated, as shown in Eq. (20).

$$F_{Ar} = v_1 \cdot \left(\frac{1}{F_{Allregion}}\right) + v_2 \cdot \left(\frac{1}{V_p}\right) + v_3 \cdot F_\theta \tag{20}$$

In the equation, $\mathcal{V}_1$, $\mathcal{V}_2$, and $\mathcal{U}_3$ referred the weight coefficients, and $v_1 + v_2 + v_3 = 1$.

*Design of the FIA*ACO algorithm*

By analyzing the requirements of the leveling operation process, the inclusion of $q\,(n)$ in the heuristic function enhanced the evaluation function of the traditional A* algorithm, as demonstrated in Eq. (21).

$$f(n) = g(n) + h(n) + q(n) \tag{21}$$

In the equation, $q\,(n)$ represented three working conditions based on the grader's load at the parent node: (1) When the grader's current load was 70% or more of its maximum capacity, filling operation was prioritized; (2) When the grader's load was at or below 30% of its maximum capacity, digging operation was given priority; (3) In all other situations, priority was given to advancing to the child node that exhibited the highest rate of change in earthwork volume compared to the parent node grid.

$$q(n) = \begin{cases} V_{c_{node}} \cdot \Gamma & V_{p_{node}} \geq 0.7 V_{max} \\ frac V_{i_{node}} V_{j_{node}} \cdot \left| \frac{V_{i_{node}} + V_{j_{node}}}{V_{i_{node}} - V_{j_{node}}} \right| & others \\ frac \Gamma V_{c_{node}} & V_{p_{node}} \leq 0.3 V_{max} \end{cases} \tag{22}$$

In the equation, $V_{p_{node}}$ denoted the load of the grader at the parent node grid, m^3; $V_{c_{node}}$ referred the load of the grader after passing the child node grid, m^3; $V_{j_{node}}$ denoted the earthwork volume to be processed at the child node grid, m^3; $V_{i_{node}}$ referred the earthwork volume to be processed at the parent node grid, m^3; $V_{\max}$ denoted the maximum load of the grader, m^3; Γ was a constant, set to 0.01 in this paper.

The initial pheromone concentration on the path was adjusted, as demonstrated in Eq. (23).

$$\tau(0) = \begin{cases} 8K & The\ path\ planned\ by\ the\ FIA*ACO \\ 8 & Other\ paths \end{cases} \tag{23}$$

In the equation, K referred the magnification factor, which was taken as 2 in this paper.

To enhance the convergence performance of the FIA*ACO, a reward-punishment mechanism was implemented to update pheromone levels, effectively guiding ants in their exploration of superior operational paths. When an ant discovered a better path, it deposited additional pheromone along the route as a reward, thereby increasing the likelihood that subsequent ants would select that path. Conversely, if an ant identified a suboptimal path, it reduced pheromone deposition as a form of punishment, thereby decreasing the chances of future ants choosing that route. Additionally, a flat terrain operation path quality coefficient was introduced to evaluate the quality of various operational paths, as detailed in Eq. (24).

$$\varrho = \frac{F_{Ar}^{\min}}{F_{Ar\ m}^{\min}} \tag{24}$$

In the equation, $\mathbf{F}_{Ar}^{\min}$ denoted the minimum value of the ant colony optimization objective function by the k-th iteration; $F_{Ar}^{\min} m$ referred the minimum value of the optimization objective function for the m-th ant by the k -th iteration.

The pheromone update that incorporated the flat terrain operation path quality coefficient was presented in Eq. (25), while the pheromone increment was detailed in Eq. (26).

$$\tau_{ij}(t+1) = (1-\rho) \cdot \tau_{ij}(t) + \sum_{m=1}^{W_{ant}} \Delta\tau_{ij}^{m}(t) \tag{25}$$

$$\Delta\tau_{ij}^{m}(t) = \varrho \cdot \frac{Q}{F_{Ar\ \ m}^{\min}} \tag{26}$$

In the equation, $\tau_{ij}\,(t+1)$ denoted the pheromone concentration between grid i and grid j at time $(t+1)$; ρ referred the pheromone evaporation factor; $\Delta\tau_{ij}^{m}(t)$ denoted the pheromone increment on the path between grid i and grid j when the m-th ant passed at time t; $\mathcal{Q}$ was a constant, set to 10 in this paper; W_{ant} referred the number of ants.

The flowchart of full-field fine-grid leveling operation path planning was shown in Fig. 4.

Results

To validate the robust global optimization capability and rapid convergence speed of the proposed IACO for inter-region path planning and the FIA*ACO for full-field precision operation path planning, simulation experiments were carried out using MATLAB. The parameters used in the algorithm were provided in Table 2. The distribution of earthwork volume in the two farmlands before levelling were presented in Fig. 5.

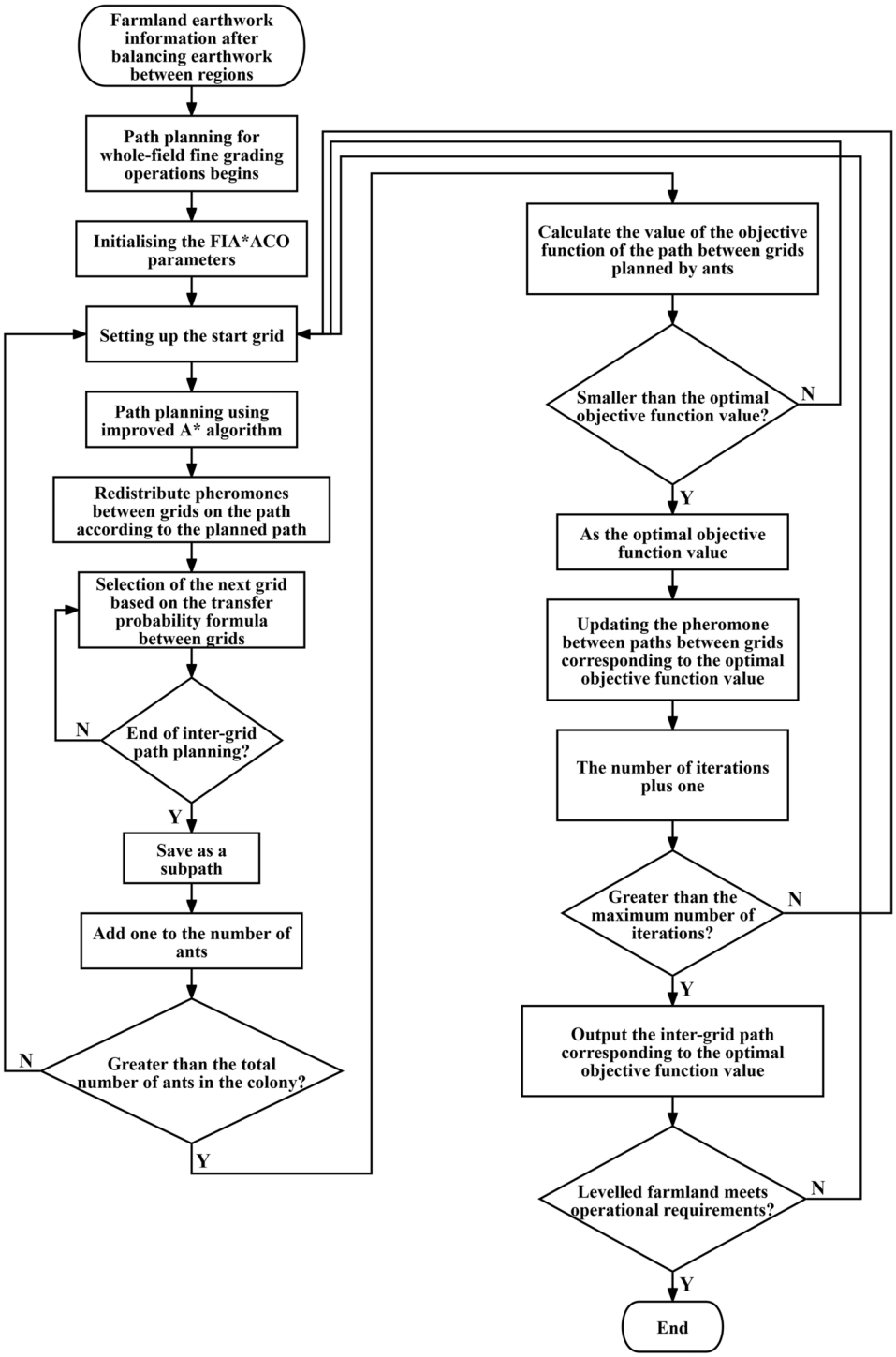

Fig. 4. Flowchart of full-field fine-grid leveling operation path planning.

Simulation test validation of inter-regional operation path planning

Performance test experiment for the IACO

The algorithm's performance impacted the path planning results, which directly affected the effectiveness of flat terrain operations. To assess the optimization capability of the IACO proposed in this paper, four test functions (categorized as unimodal and multimodal) listed in Table 3 were utilized to evaluate the IACO algorithm's performance in terms of convergence speed, accuracy, and global optimization.

The performance results from the simulation test were displayed in Table 4. Analysis of the table indicated that the optimal value, average value, and standard deviation of the proposed IACO were significantly superior to those of the ACO when solving both unimodal and multimodal functions.

Parameters	Values
Maximum load capacity of the scraper $V_{\max}/m^3$	2.5
Weight coefficient of the inter-regional operation path optimization function ω_1	0.6
Weight coefficient of the inter-regional operation path optimization function ω_2	0.4
Pheromone weight factor α	2
Heuristic function weight factor β	4
Maximum number of iterations $k_{\max}$/times	100
Constant Q_1	2
Pheromone evaporation factor ρ	0.5
Weight coefficient of pheromone evaporation factor ρ_a	0.95
Minimum value of pheromone evaporation factor $\rho_{\min}$	0.4
Pheromone intensity coefficient Q	10
Upper limit of the pheromone $\tau_{\max}$	45
Lower limit of the pheromone $\tau_{\min}$	2
Weight coefficient of the full-field precision operation path optimization function υ_1	0.3
Weight coefficient of the full-field precision operation path optimization function $\mathcal{V}_2$	0.4
Weight coefficient of the full-field precision operation path optimization function $\mathcal{V}_3$	0.3

Table 2. Parameters and their values involved in the improved ant colony optimization algorithm.

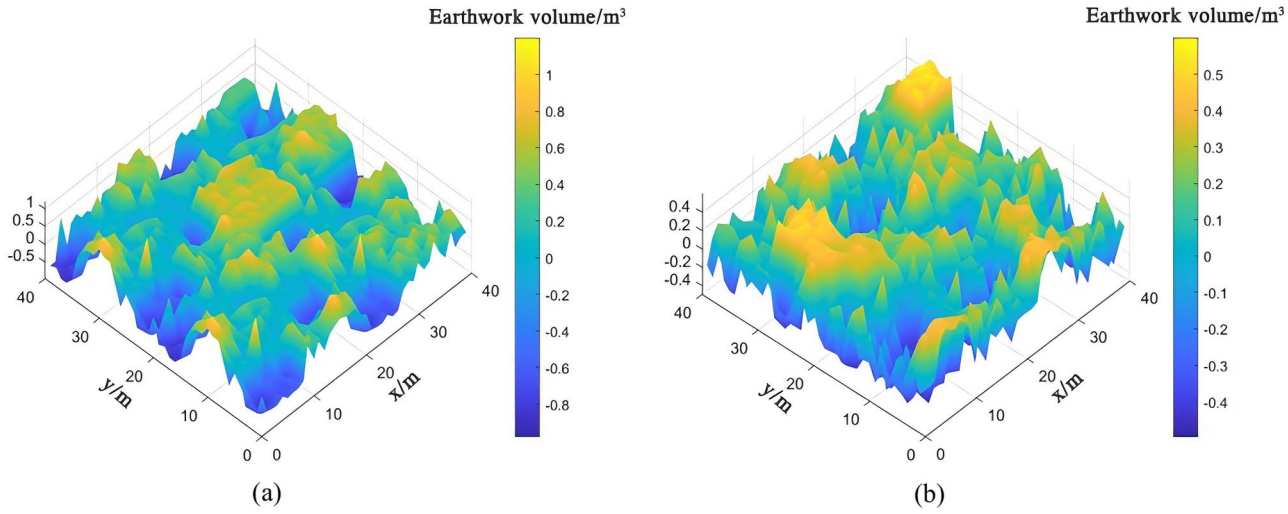

Fig. 5. Information on the earthwork volume distribution of farmland before levelling. (**a**) 3D distribution of earthwork volume infarmland 1 before levelling. (**b**) 3D distribution of earthwork volume infarmland 2 before levelling.

Name	Expression	Variable range
Sphere	$F_1(x) = \sum_{i=1}^{n} x_i^2$	[−100,100]
Schwefel 2.22	$F_2(x) = \sum_{i=1}^{n} \lvert x_i \rvert + \prod_{i=1}^{n} \lvert x_i \rvert$	[−10,10]
Rastrigin	$F_3(x) = \sum_{i=1}^{n} \left[x_i^2 - 10\cos(2\pi x_i) + 10 \right]$	[−5.12,5.12]
Ackley	$F_4(x) = -20\exp\left(-0.2\sqrt{\frac{1}{n}\sum_{i=1}^{n} x_i^2}\right) - \exp\left(\frac{1}{n}\sum_{i=1}^{n}\cos(2\pi x_i)\right)$	[−32,32]

Table 3. Four test functions.

Function name	Algorithm name	Optimal value	Average value	Worst value	Standard deviation
$F_1(x)$	ACO	1.6467e−14	0.3665	9.5641	1.2962
	IACO	9.4902e−43	0.1024	8.1807	0.8284
$F_2(x)$	ACO	4.2348e−11	56.0354	438.6704	95.5825
	IACO	2.2737e−13	17.9673	304.2203	66.0945
$F_3(x)$	ACO	0.077689	1.1423	48.0121	5.8534
	IACO	0.013438	3.5006	92.4867	14.2206
$F_4(x)$	ACO	5.4179e−14	0.2524	8.8645	1.2938
	IACO	8.8817e−16	2.1467e−04	0.0022	6.2666e−04

Table 4. Performance test results based on the ACO and IACO.

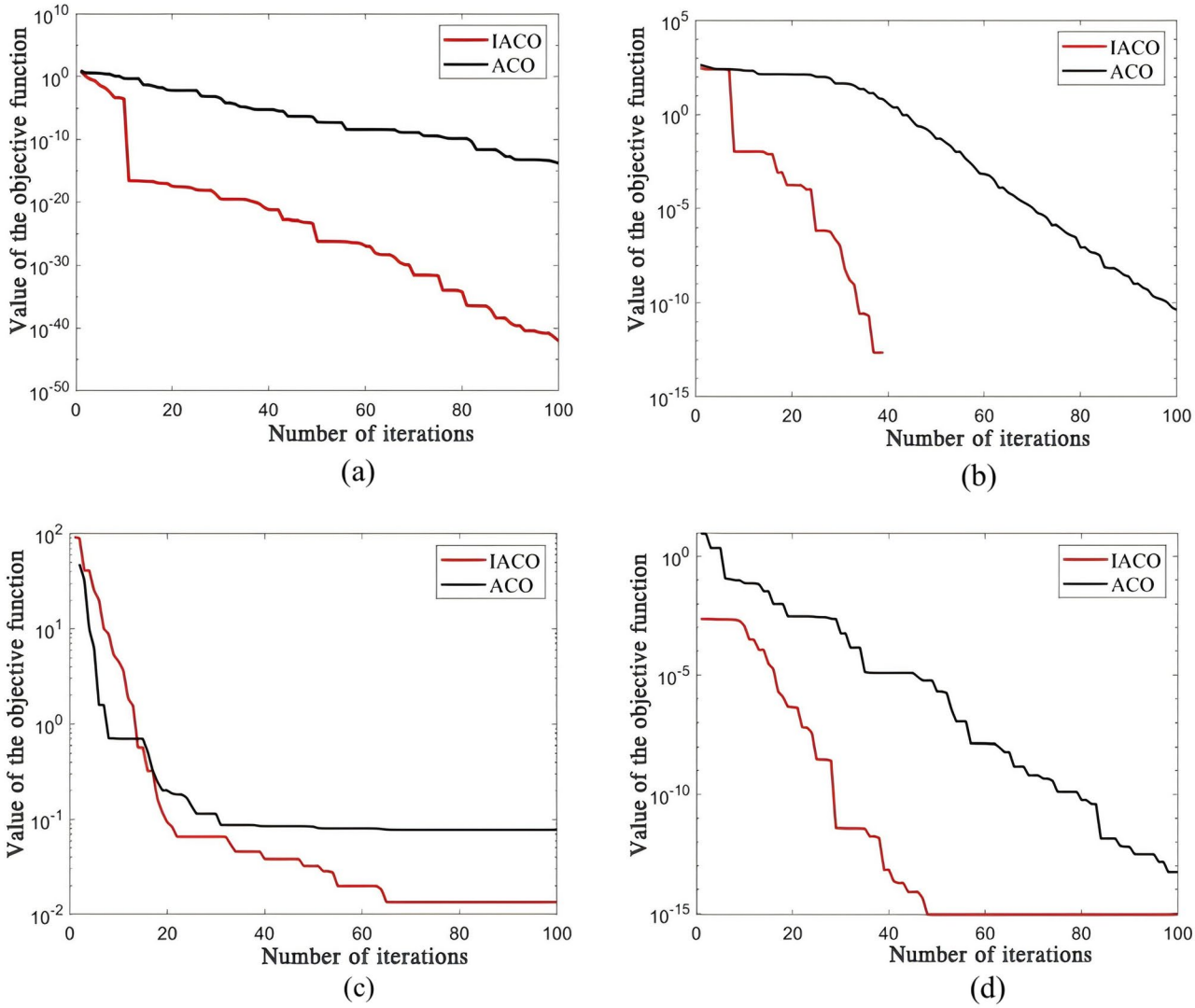

Fig. 6. The convergence processes of four functions to the optimal solution based on the ACO and IACO. (**a**) $F_1(x)$ converged to the optimal solutionbased on the ACO and IACO. (**b**) $F_2(x)$ converged to the optimal solutionbased on the ACO and IACO. (**c**) $F_3(x)$ converged to the optimal solutionbased on the ACO and IACO. (**d**) $F_4(x)$ converged to the optimal solutionbased on the ACO and IACO.

The process of four functions converging to the optimal solution using the ACO and IACO were illustrated in Fig. 6. Analysis of the figures indicated that the IACO developed in this paper significantly outperformed the ACO in terms of convergence speed, accuracy, and global optimization, validating the effectiveness of the improvements made to the heuristic function and pheromone update strategy in the ACO.

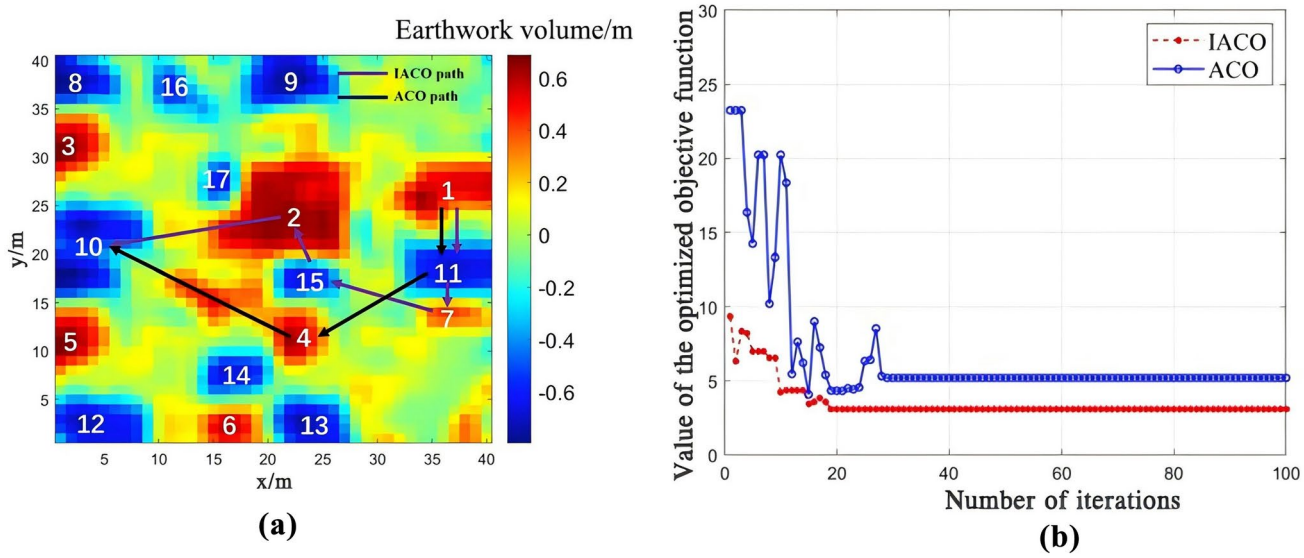

Fig. 7. Path planning and objective function convergence curve of farmland 1 based on the ACO and IACO. (**a**) Optimal inter-region operational path based on the ACO and IACO. (**b**) Convergence curve of the optimization objective function based on the ACO and IACO.

Name of search algorithm	Optimal operational path sequence between regions in farmland 1
ACO	1 → 11 → 4 → 10
IACO	1 → 11 → 7 → 15 → 2 → 10

Table 5. Optimal operational path sequences between regions in farmland 1 based on the ACO and IACO.

Simulation analysis of operation path planning with the same start and end regions

(1) Path planning for farmland 1.

In the first inter-region path planning, the region near the edge of the farmland with the largest amount of earthwork volume to be excavated was selected as the starting region, and the region with the largest amount of earthwork volume to be filled was selected as the ending region for inter-region path search. As shown in Fig. 7a, Region 1 was set as the starting region, and region 10 was set as the ending region. The purple path represented the search path of the IACO, while the black path represented the search path of the ACO. For inter-region path planning in farmland 1, the convergence curves of different algorithms were presented in Fig. 7b, and the final path planning results were presented in Table 5. The simulation results indicated that, compared with the ACO, the IACO reduced the iterations to convergence by 31.75%, and the value of the optimized objective function after convergence was reduced by 47%.

Figure 8a presented the optimal operational path planned by the ACO within farmland 1, and Fig. 8b presented the optimal operational path planned by the IACO within farmland 1. The path started from the starting region, passed through intermediate node regions, and finally reached the ending region. According to the simulation results, the ACO only optimized for the shortest inter-region operational distance, which did not reflect the actual flat terrain work condition. In contrast, the IACO generated a path that better fit the flat terrain work scenario, fully considering both inter-region distance and the volume of earthwork to be done between regions.

The evaluation indicators of the optimal operational paths planned by the algorithms mentioned above were presented in Table 6. The analysis indicated that, compared to the ACO, the IACO reduced empty load travel distance by 19.7% and increased the efficiency of earthwork volume movement by over 50%.

(2) Path planning for farmland 2.

The optimal inter-regional operational path search and planning for farmland 2, based on the ACO and IACO, were presented in Fig. 9a. Region 1 was set as the starting point, and region 8 was set as the ending point. The optimal inter-regional operational path sequences planned by the ACO and IACO were presented in Table 7. Analysis of Fig. 9b indicated that, compared with the ACO, the IACO reduced the number of convergence iterations by 40% and decreased the value of the optimized objective function by 31.7%.

Figure 10a presented the optimal operational path planned by the ACO within farmland 2, and Fig. 10b presented the optimal operational path planned by the IACO within farmland 2.

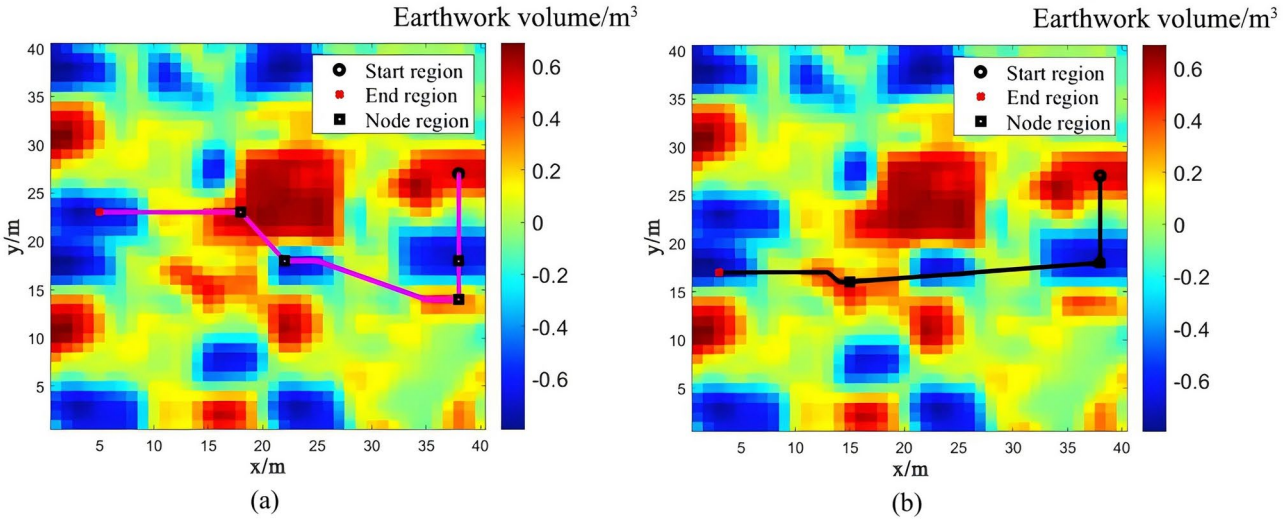

Fig. 8. Optimal inter-region operational path planning of farmland 1 based on the ACO and IACO. (**a**) Optimal inter-region operational path searched and planned based on the ACO. (**b**) Optimal inter-region operational path searched and planned based on the IACO.

Search and planning algorithm	Total path length/m	Empty load travel distance/m	Volume of earthwork moved/m³
ACO	136.2	86.97	3.15
IACO	147.51	65.51	7.2

Table 6. Evaluation indicators of the optimal operational paths for farmland 1 searched and planned based on the ACO and IACO.

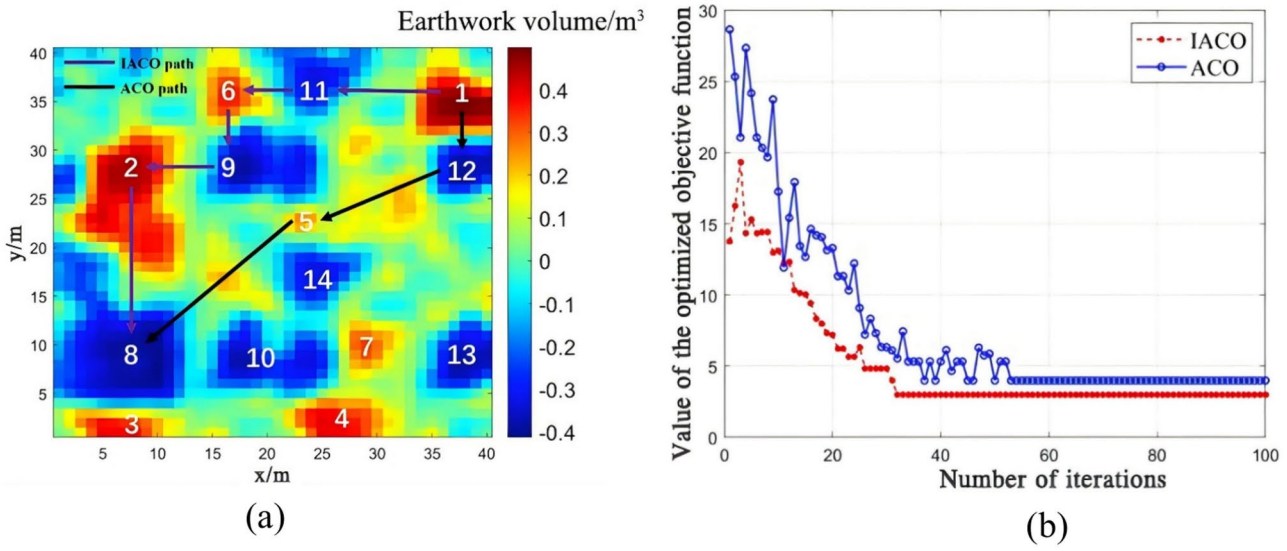

Fig. 9. Path planning and objective function convergence curve of farmland 2 based on the ACO and IACO. (**a**) Optimal inter-region operational path based onthe ACO and IACO. (**b**) Convergence curve of the optimizationobjective function based on the ACO andIACO.

The evaluation indicators for the optimal operational paths planned by the algorithms mentioned above were presented in Table 8. Analysis indicated that, compared with the ACO, the IACO reduced empty load travel distance by 17.3% and increased the efficiency of earthwork volume movement by more than 30%.

Through the analysis of the optimal operational path search and planning for two farmlands with different earthwork distributions and topographies, it was evident that the IACO not only optimized for the shortest

Name of search algorithm	Optimal operational path sequence between regions in farmland 2
ACO	1 → 12 → 5 → 8
IACO	1 → 11 → 6 → 9 → 2 → 8

Table 7. Optimal operational path sequences between regions in farmland 2 based on the ACO and IACO.

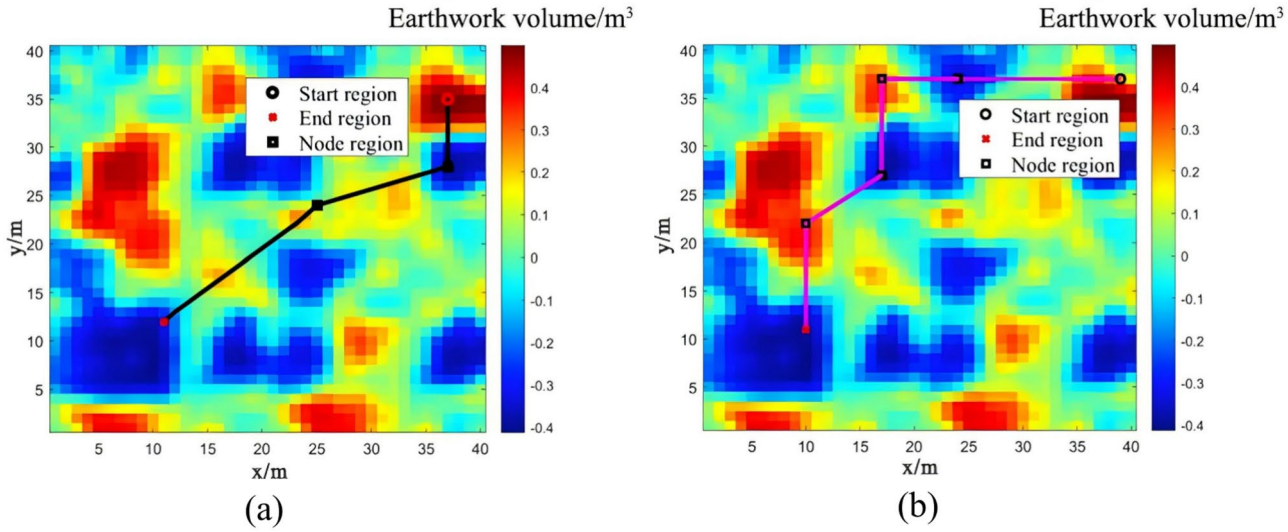

Fig. 10. Optimal inter-region operational path planning of farmland 2 based on the ACO and IACO. (**a**) Optimal inter-region operational pathsearched and planned based on the ACO. (**b**) Optimal inter-region operational pathsearched and planned based on the IACO.

Search and planning algorithm	Total path length/m	Empty load travel distance/m	Volume of earthwork moved/m³
ACO	114.37	69.27	3.15
IACO	155.01	67.07	6.2

Table 8. Evaluation indicators of the optimal operational paths for farmland 2 searched and planned the ACO and IACO.

Search and planning algorithm	Empty load rate/%	Full load rate/%	Total path length/m	Empty load travel distance/m	Remaining earthwork volume/m³	Number of paths
ACO	19.1	21.4	4600.34	2214.3	115.56	78
IACO	2.1	2.3	3445.30	1030.5	112.31	63

Table 9. Evaluation indicators of the optimal operation path in farmland 1 searched and planned based on the ACO and IACO.

operational distance but also integrated both operational distance and the volume of earthwork between regions. For the same starting and ending regions, the IACO significantly reduced empty load travel distance and increased the efficiency of earthwork volume movement during inter-region path planning.

Simulation analysis of inter-regional earthwork balance operation path planning

The above experiment only analyzed single-instance inter-region operational path planning. Although the IACO algorithm's advantages were demonstrated, the analysis remained incomplete. Therefore, it was necessary to use both the ACO and IACO to complete the earthwork balance operations between regions and analyze the overall operational effect to further highlight the advantages of the IACO.

(1) Simulation analysis of operation path planning in farmland 1.

The evaluation indicators after complete levelling operations between regions in farmland 1 were presented in Table 9. According to the simulation results, compared to the ACO, the IACO reduced the empty load rate by

17%, decreased the full load rate by 19.1%, reduced the total path length by 25.1%, and lowered empty load travel distance by 53.46%. Therefore, from the overall analysis of operational effectiveness, the levelling operation based on the IACO proved to be more efficient.

The remaining earthwork volume after complete levelling operations between regions in farmland 1, based on the ACO and IACO, were presented in Fig. 11. Figure 11a, b were the 3D information graphs of the remaining earthwork volume after complete levelling operations using the ACO and IACO, respectively. Figure 11c, d were the corresponding 2D information graphs. From the analysis of the figures, it could be observed that the remaining earthwork volume was lower, and the terrain was smoother after complete levelling operations between regions in farmland 1 based on the IACO.

(2) Simulation analysis of operation path planning in farmland 2.

The evaluation indicators after complete levelling operations between regions in farmland 2 were presented in Table 10. According to the simulation results, compared to the ACO, the IACO reduced the empty load rate by 16.6%, decreased the full load rate by 19.65%, reduced the total path length by 29.9%, and lowered empty load travel distance by 36.55%. Therefore, from the overall analysis of operational effectiveness, the levelling operation based on the IACO proved to be more efficient.

The remaining earthwork volume after levelling operations between regions in farmland 2, based on the ACO and IACO, were presented in Fig. 12. Figure 12a, b represented the 3D information graphs of the remaining earthwork volume after levelling operations using the ACO and IACO, respectively. Figure 12c, d were the corresponding 2D information graphs. From the simulation results, it could be observed that for farmland with

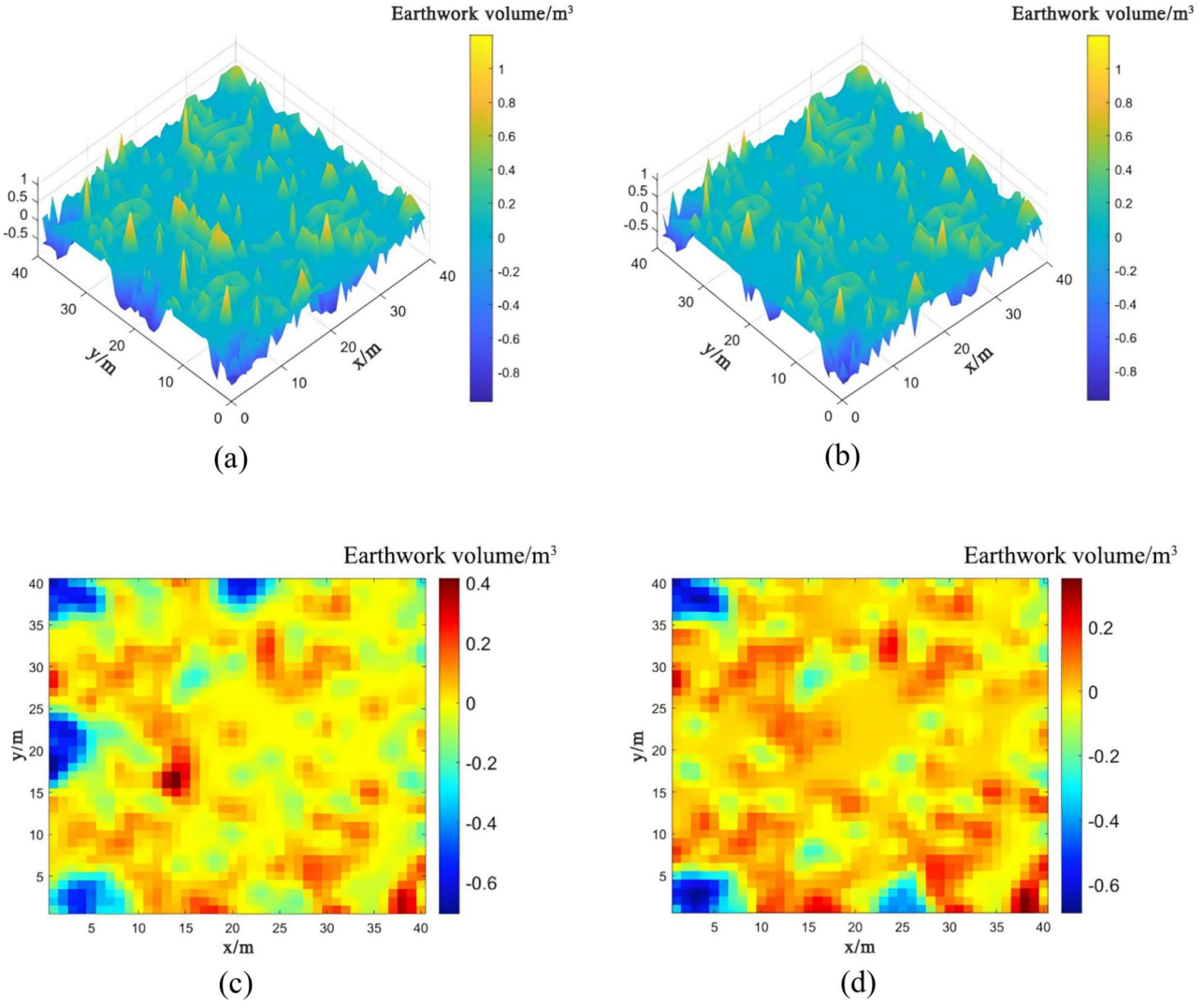

Fig. 11. Information on remaining earthwork volume after complete levelling operations between regions in farmland 1 based on the ACO and IACO. (**a**) 3D information of remaining earthworkvolume based on the ACO. (**b**) 3D information of remaining earthworkvolume based on the IACO. (**c**) 2D information of remaining earthworkvolume based on the ACO. (**d**) 2D information of remaining earthworkvolume based on the IACO.

Search and planning algorithm	Empty load rate/%	Full load rate/%	Total path length/m	Empty load travel distance/m	Remaining earthwork volume/m³	Number of paths
ACO	18.4	22.3	4226.67	2082.2	102.9	48
IACO	1.8	2.65	2961.32	1323.3	98.4	41

Table 10. Evaluation indicators of the optimal operation path in farmland 2 searched and planned based on the ACO and IACO.

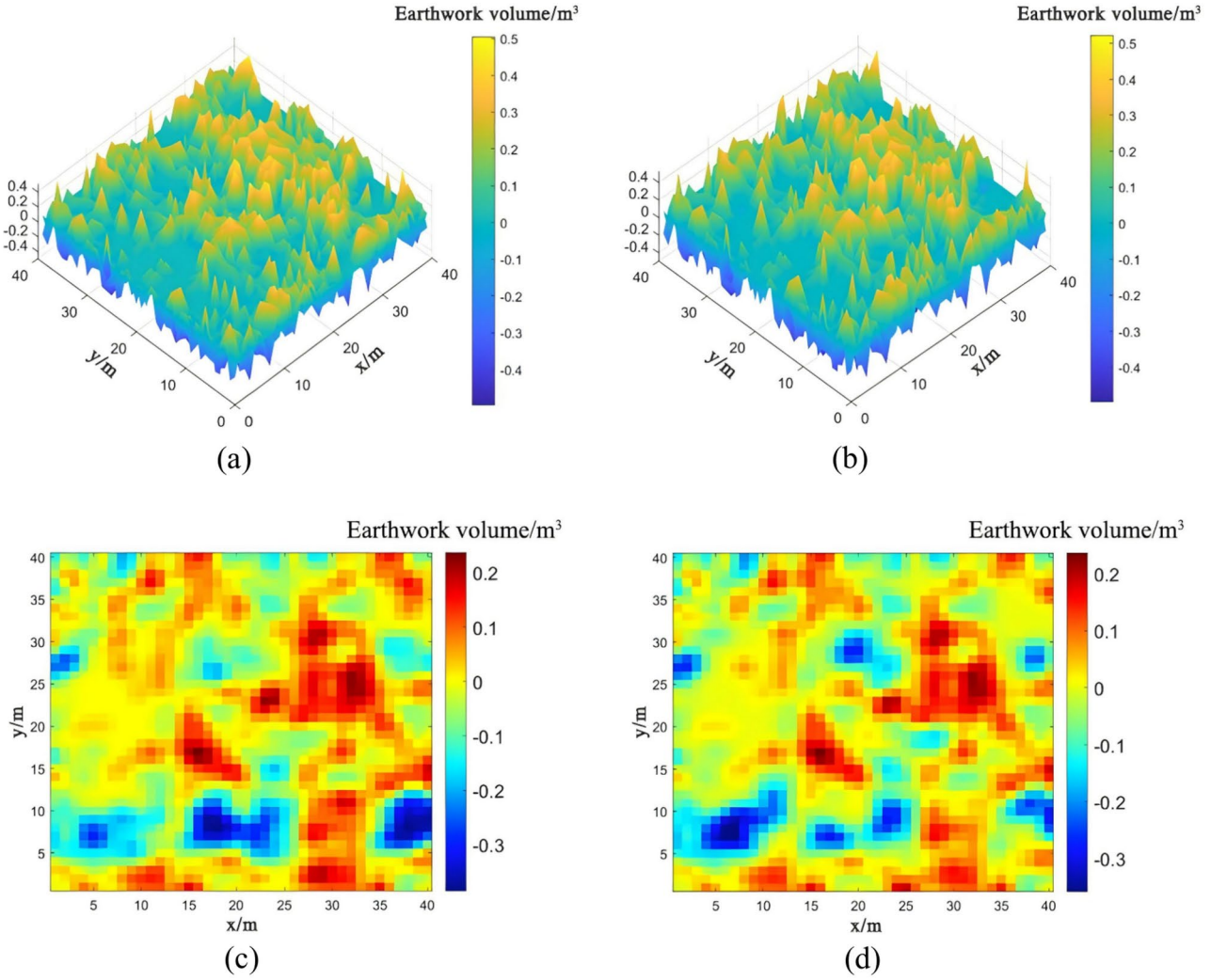

Fig. 12. Information on remaining earthwork volume after complete levelling operations between regions in farmland 1 based on the ACO and IACO. (**a**) 3D information of remaining earthwork volume based on the ACO. (**b**) 3D information of remaining earthwork volume based on the IACO. (**c**) 2D information of remaining earthwork volume based on the ACO. (**d**) 2D information of remaining earthwork volume based on the IACO.

small terrain undulations, the earthmoving efficiency in complete levelling operations between regions based on the IACO was higher.

From the analysis of the above simulation results, it could be observed that the designed IACO demonstrated high operational efficiency and an effective levelling performance when working on farmland with varying terrains.

Simulation test validation of full-field precision operation path planning

*Performance test experiment for the FIA*ACO*

The experiment compared the performance of three different ant colony optimization algorithms applied to four typical test functions. The experimental results were presented in Table 11.

Name of function	Name of algorithm	Optimal value	Average value	Worst value	Standard deviation
$F_1(x)$	ACO	6.1754e−08	3.5708e+11	3.5708e+13	3.5708e+12
	IACO	1.3852e−43	0.8386	40.9261	4.8509
	FIA*ACO	2.8027e−80	0.0290	1.6504	0.1871
$F_2(x)$	ACO	8.4981e−11	63.0094	443.1761	97.2997
	IACO	4.7180e−12	1.7670	165.9505	16.5871
	FIA*ACO	5.6843e−14	0.4303	31.3961	3.3355
$F_3(x)$	ACO	0.0323	1.5325	45.5520	6.3442
	IACO	0.00731	3.1507	88.9737	13.5705
	FIA*ACO	5.2393e−04	0.0044	0.0927	0.0182
$F_4(x)$	ACO	6.4943e−10	1.3433	20.7071	3.7802
	IACO	8.88178e−16	0.5979	20.5132	2.9491
	FIA*ACO	8.8818e−16	8.8025e−04	0.0226	0.0043

Table 11. Performance of four test functions based on the ACO, IACO, and FIA*ACO.

From the analysis of the table results, it could be observed that, compared with the other three ant colony optimization algorithms, the FIA*ACO designed in this paper performed better in terms of convergence accuracy and solution stability when solving the first three test functions. Although the convergence accuracy was slightly lower than that of the IACO when solving the fourth test function, its solution stability was thousands of times higher.

The process of convergence to the optimal solution for the four functions, based on the ACO, IACO, and FIA*ACO, were shown in Fig. 13. From the analysis of the figures, it was evident that the FIA*ACO demonstrated a faster convergence speed when solving both unimodal and multimodal functions.

Simulation analysis of operation path planning with the same start and end grids

(1) Path planning for farmland 1.

In farmland 1, the path planning started from the grid coordinates (38.1) with a grid earthwork volume of 0.45 and ended at the grid coordinates (4.38) with a grid earthwork volume of −0.69. The optimal path planning based on the ACO and FIA*ACO were shown in Fig. 14a. Figure 14b presented the corresponding convergence curve of the optimization objective function value. From the analysis of the simulation results, it could be observed that, compared with the ACO, the FIA*ACO increased the convergence speed by 74% and reduced the optimization objective function value by 26.3%.

The specific evaluation indicators and values for the optimal planned operation path of farmland 1, based on different algorithms, were presented in Table 12. From the table, it could be observed that, when the total path length difference was small, compared with the ACO, the operation path planned by the FIA*ACO reduced the empty and full load rate by 12%, decreased the turning objective function value by 66.7%, and increased the efficiency of earthwork volume movement by 47.37%.

(2) Path planning for farmland 2.

In farmland 2, the path planning started from the grid coordinates (36,40) with a grid earthwork volume of 0.66 and ended at the grid coordinates (7,8) with a grid earthwork volume of −0.59. The optimal path planning based on the ACO and FIA*ACO were shown in Fig. 15a. Figure 15b presented the corresponding convergence curve of the optimization objective function value. From the analysis of the simulation results, it could be observed that, compared with the ACO, the FIA*ACO increased the convergence speed by 63% and reduced the optimization objective function value by 24.8%.

The specific evaluation indicators and values for the optimal planned operation path of farmland 2, based on different algorithms, were presented in Table 13. From the table, it could be observed that, compared with the ACO, the operation path planned by the FIA*ACO reduced the empty and full load rate by 14.95%, decreased the turning objective function value by 65.38%, increased the efficiency of earthwork volume movement by 50.9%, and resulted in a greater cumulative sum of the load variation rate for the grader.

From the analysis of the above simulation test results, it could be observed that the FIA*ACO significantly reduced the empty and full load rate and the number of steering times, while increasing the volume of earthwork moved and the cumulative sum of the load variation rate for the grader in the planning of the single operation path.

Simulation analysis of full-field precision levelling operation path planning

(1) Path planning for farmland 1.

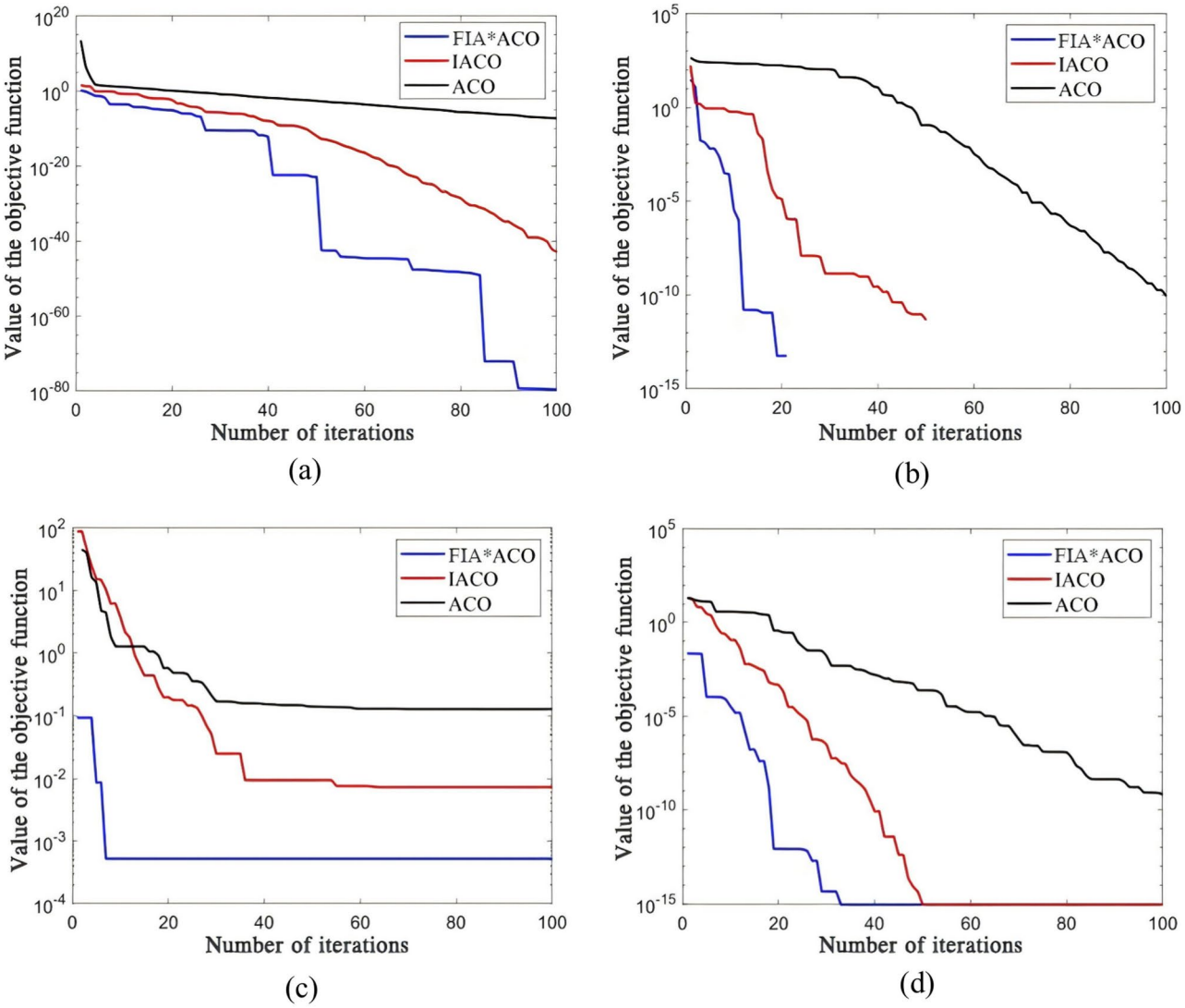

Fig. 13. The process of four functions converging to the optimal solution based on the ACO, IACO, and FIA*ACO. (**a**) $F_1(x)$ converged to the optimal solutionbased on the ACO, IACO, and FIA*ACO. (**b**) $F_2(x)$ converged to the optimal solutionbased on the ACO, IACO, and FIA*ACO. (**c**) $F_3(x)$ converged to the optimal solutionbased on the ACO, IACO, and FIA*ACO. (**d**) $F_4(x)$ converged to the optimal solutionbased on the ACO, IACO, and FIA*ACO.

The distribution of earthwork volume after the complete levelling operation of farmland 1, based on different algorithms, were presented in Fig. 16. From the analysis of the simulation results, it could be observed that the remaining earthwork volume after the complete levelling operation using the FIA*ACO was significantly lower.

The specific evaluation indexes and values for the fully levelled operation paths in farmland 1, based on different algorithms, were presented in Table 14. From the analysis of the table, it could be observed that, compared with the ACO, the operation path based on the FIA*ACO resulted in a 15.9% reduction in the empty and full load rate, a 29% reduction in total path length, a 28.2% reduction in the total number of paths, and a lower remaining earthwork volume after the operation.

(2) Path planning for farmland 2.

The distribution of the remaining earthwork volume after the complete levelling operation of farmland 2, based on different algorithms, were presented in Fig. 17. From the analysis of the simulation results, it could be observed that the levelness of the farmland was significantly improved after the complete levelling operation using the FIA*ACO.

The specific evaluation indexes and values for the fully levelled operation paths in farmland 2, based on different algorithms, were presented in Table 15. From the analysis of the table, it could be observed that, compared with the ACO, the operation path based on the FIA*ACO resulted in a 10.66% reduction in the empty and full load rate, a 27.9% reduction in total path length, and a 32.6% reduction in the total number of paths.

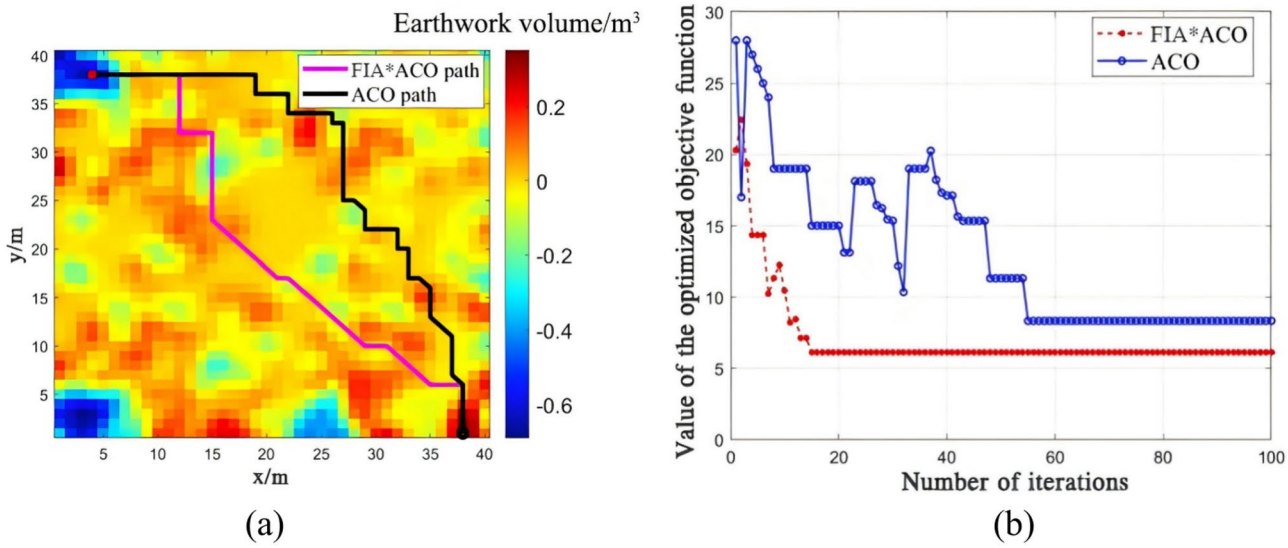

Fig. 14. Optimal path planning and convergence curve of the objective function value for farmland 1 based on the ACO and FIA*ACO. (**a**) Optimal path planning based on the ACO andFIA*ACO. (**b**) Convergence curve of the objective functionvalue based on the ACO and FIA*ACO.

Search and planning algorithm	Empty and full load rate/%	Cumulative sum of the load variation rate for the grader	Turning objective function value	Total path length/m	Volume of earthwork moved/ m^3
ACO	13.2	23	34	198.21	3.31
FIA*ACO	1.2	45	14	183.12	6.29

Table 12. Specific evaluation indicators and values for the optimal planned operation path in farmland 1 based on the ACO and FIA*ACO.

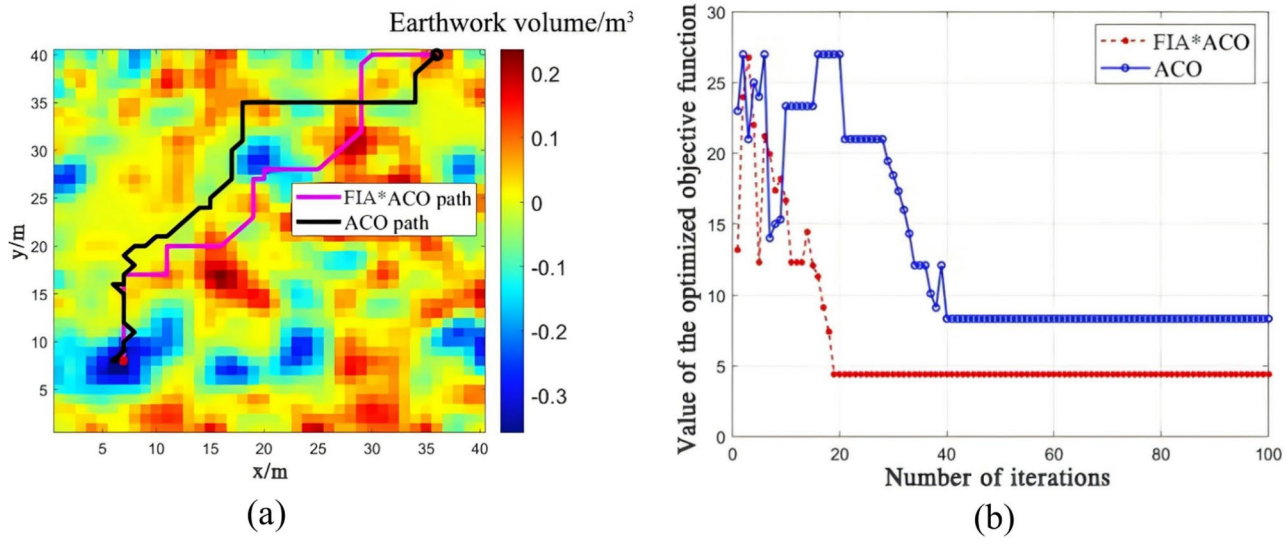

Fig. 15. Optimal path planning and convergence curve of the objective function value for farmland 2 based on the ACO and FIA*ACO. (**a**) Optimal path planning based on the ACO andFIA*ACO. (**b**) Convergence curve of the objective functionvalue based on the ACO and FIA*ACO.

Search and planning algorithm	Empty and full load rate/%	Cumulative sum of the load variation rate for the grader	Turning objective function value	Total path length/m	Volume of earthwork moved/ m^3
ACO	19.8	34	33	178.82	2.61
FIA*ACO	4.85	52	18	168.93	5.32

Table 13. Specific evaluation indicators and values for the optimal planned operation path in farmland 2 based on the ACO and FIA*ACO.

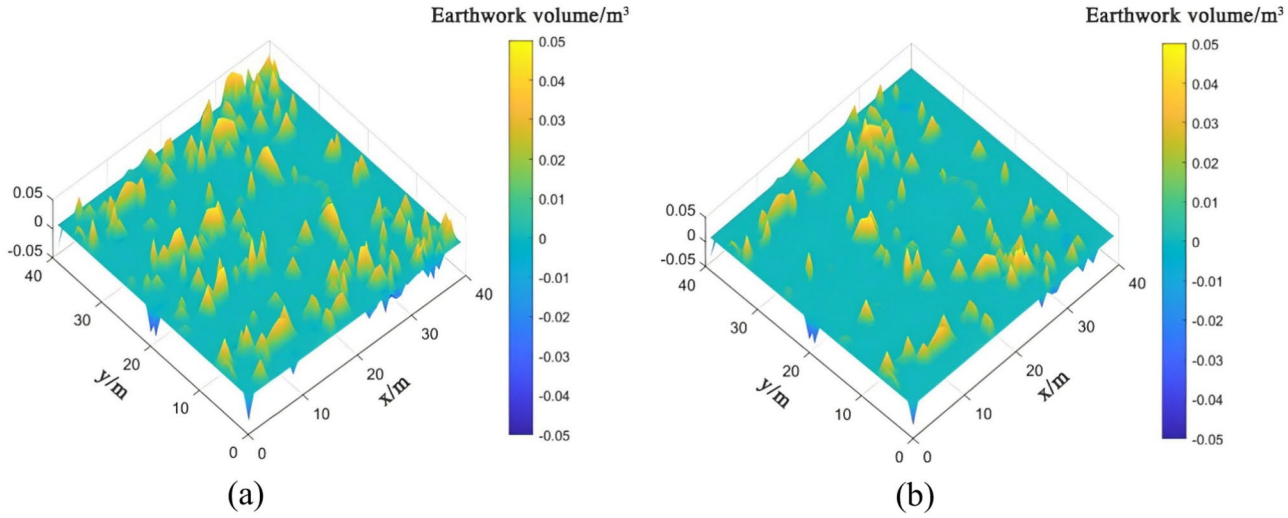

Fig. 16. Distribution of remaining earthwork volume after refined complete levelling operation for the whole field of farmland 1 based on the ACO and FIA*ACO. (**a**) Distribution of remaining earthwork volumeafter complete levelling operations based on theACO. (**b**) Distribution of remaining earthwork volumeafter complete levelling operations based on theFIA*ACO.

Search and planning algorithm	Empty and full load rate/%	Total path length/m	Total number of paths	Remaining earthwork volume/m^3
ACO	23	16,145	156	2.21
FIA*ACO	7.1	11,423	112	1.04

Table 14. Specific evaluation indexes and values of the completely levelled operation paths for farmland 1 based on the ACO and FIA*ACO.

Additionally, the remaining earthwork volume after the operation with the FIA*ACO was only 35% of that with the ACO.

In summary, when the entire field underwent refined levelling operations using the FIA*ACO, the empty and full load rate was reduced by approximately 10%, the total path length was shortened by around 28%, and the total number of paths decreased by at least 28%. These results satisfied the requirements for full-field refinement following inter-regional earthwork balancing operations.

Analysis of field experiments

To validate the effectiveness of the variable scale levelling path planning method based on the improved ant colony algorithm designed in this study, a test field provided by Jiangsu Rungu Agricultural Technology Co., Ltd. was selected for a practical field levelling operation analysis. The test field, located at 32°07′39.34494″N and 119°43′45.15670″E, is a plowed area with significant terrain undulations, covering an area of about 15.68 acres, as shown in Fig. 18. The average elevation of the test field prior to levelling was 10.0615 m. The pre-levelling elevation data generated from UAV were imported into a visualization platform to generate both an inter-regional operation path and a refined operation path[23–25], which were subsequently loaded into the automated grader platform for levelling operations. The elevation data at sampling points along the paths, before and after the operation, were measured separately. The flatness of the sampling points, the distribution of the 5 cm elevation difference, and the maximum elevation difference were employed as the main evaluation indicators to assess the optimization effectiveness of the operation paths.

Method for calculating flatness:

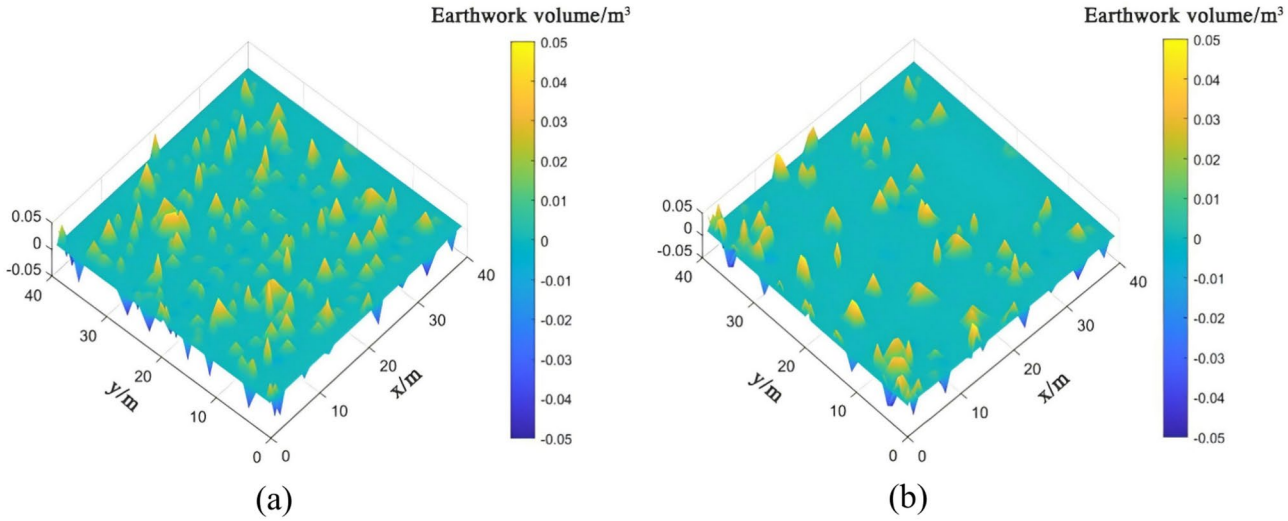

Fig. 17. Distribution of the remaining earthwork volume after refined complete levelling operation for the whole field of farmland 2 based on the ACO and FIA*ACO. (**a**) Distribution of the remaining earthworkvolume after complete levelling operationsbased on the ACO. (**b**) Distribution of the remaining earthworkvolume after complete levelling operationsbased on the FIA*ACO.

Search and planning algorithm	Empty and full load rate/%	Total path length/m	Total number of paths	Remaining earthwork volume/m³
ACO	18	13,467	138	3.77
FIA*ACO	7.34	9704	93	1.32

Table 15. Specific evaluation indexes and values of the completely levelled operation paths for farmland 2 based on the ACO and FIA*ACO.

Fig. 18. Test field before leveling.

$$S_d = \sqrt{\frac{\sum_{i=1}^{n}(h_i - h_{ave})^2}{(n-1)}} \tag{27}$$

In the equation, S_d represented flatness, m; n denoted the number of sampling points; h_i referred the elevation of the sampling points, m; h_{ave} represented the average elevation of all sampling points along the path, m.

The distribution of the 5 cm elevation difference pertained to the ratio of sampling points whose elevation deviated from the reference elevation by ± 5 cm, relative to the total number of sampling points. This metric served as an indicator of the uniformity of the farm's elevation.

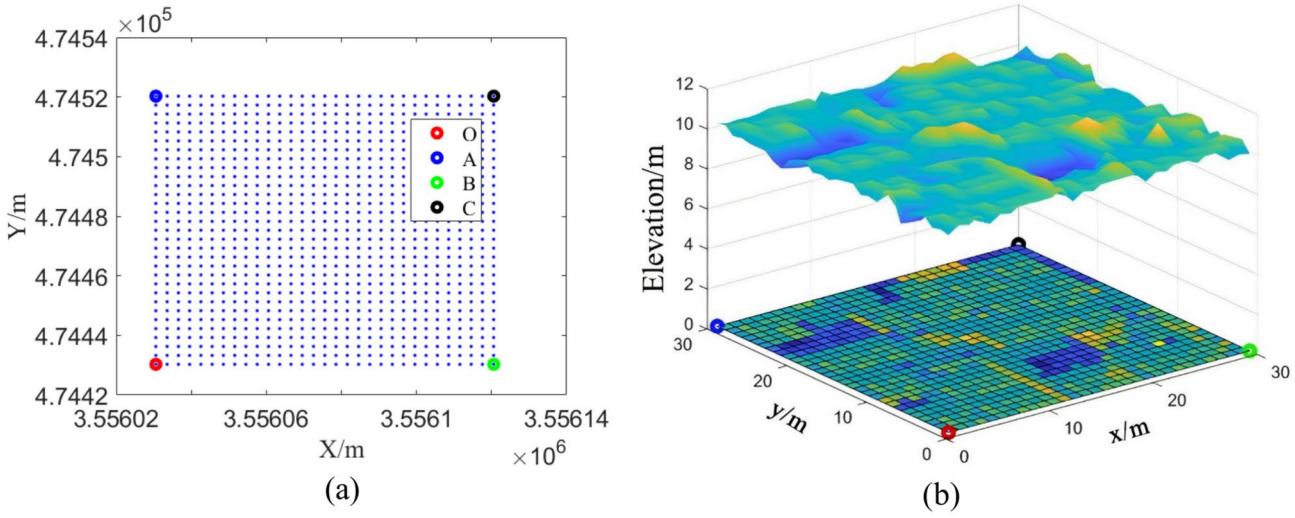

Fig. 19. Different coordinates of the field. (**a**) Gaussian coordinates of the field. (**b**) Cartesian coordinates of the field.

Boundary points	Gaussian X coordinate value	Gaussian Y coordinate value	Cartesian x coordinate value	Cartesian y coordinate value
O	3,556,030.574	474,430.279	0	0
A	3,556,030.574	474,520.279	0	31
B	3,556,120.574	474,430.279	31	0
C	3,556,120.574	474,520.279	31	31

Table 16. Gaussian and Cartesian coordinates of field boundary points.

Method for calculating maximum elevation difference:

$$H_{\max} = \max\left(|h_i - h_{\text{ave}}|\right) \tag{28}$$

In the equation, $H_{\max}$ represented the maximum elevation difference, m.

The Gaussian coordinates of the test field after rasterization were shown in Fig. 19a, b showed the corresponding Cartesian coordinates. By determining the Gaussian and Cartesian coordinates of the four vertices of the field, the Cartesian coordinate of any point within the field could be converted to the Gaussian coordinate using Eq. (29). On the visualization platform, the Cartesian coordinates of the path nodes were converted to the corresponding Gaussian coordinates. O, A, B, and C represented the four vertices of the rectangular field.

$$\begin{cases} X = (x-1) * 3 + 3556030.574 & x \geq 1 \\ Y = (y-1) * 3 + 474430.279 & y \geq 1 \end{cases} \tag{29}$$

In the equation, X and Y represented Gaussian coordinates, while $\mathcal{X}$ and y denoted Cartesian coordinates.

The Gaussian and Cartesian coordinates of the four boundary points O, A, B, and C were shown in Table 16.

Validation experiment of inter-regional operation path planning effectiveness

This experiment analyzed the levelling effectiveness of the inter-regional operation path planned using the IACO algorithm. The inter-regional operation path of the test field was planned using the visualization platform, with the start coordinates (3, 25, 0.41) and the end coordinates (27, 15, −0.54), as shown in Fig. 20. According to Eq. (29), the conversion from Gaussian coordinates to Cartesian coordinates of the field was carried out.

The elevation information of grid nodes along the inter-regional path before and after the operation was shown in Fig. 21a, and it was converted into earthwork volume information as shown in Fig. 21b. Analysis of the figure showed that the ideal earthwork volume for the planned inter-regional path should be 2.91 m^3, while the actual levelling earthwork volume was 2.57 m^3. The ratio of actual to ideal earthwork volume was 88.3%, indicating that the planned inter-regional path met the requirements for practical field levelling operations.

The evaluation indicator values of the inter-regional path before and after levelling were shown in Table 17. Analysis of the table showed that after the inter-regional levelling operation, the maximum elevation difference of the path decreased by 47.5%, the distribution of the 5 cm elevation difference increased by 26.3%, and the flatness improved by 53.7%. The planned inter-regional path demonstrated good levelling effectiveness, meeting the requirements for practical levelling operations.

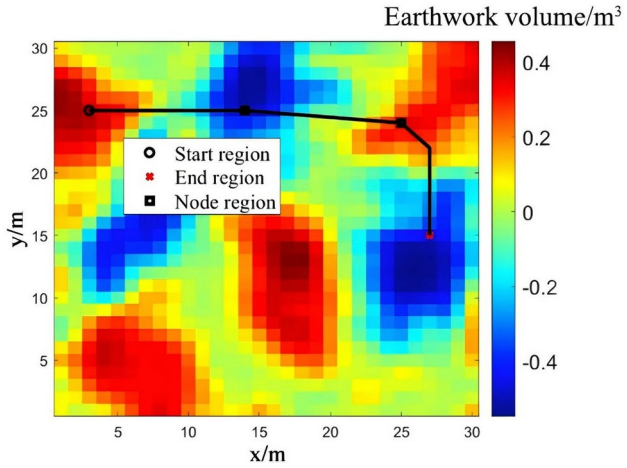

Fig. 20. Inter-regional operation path planning based on the visualization platform.

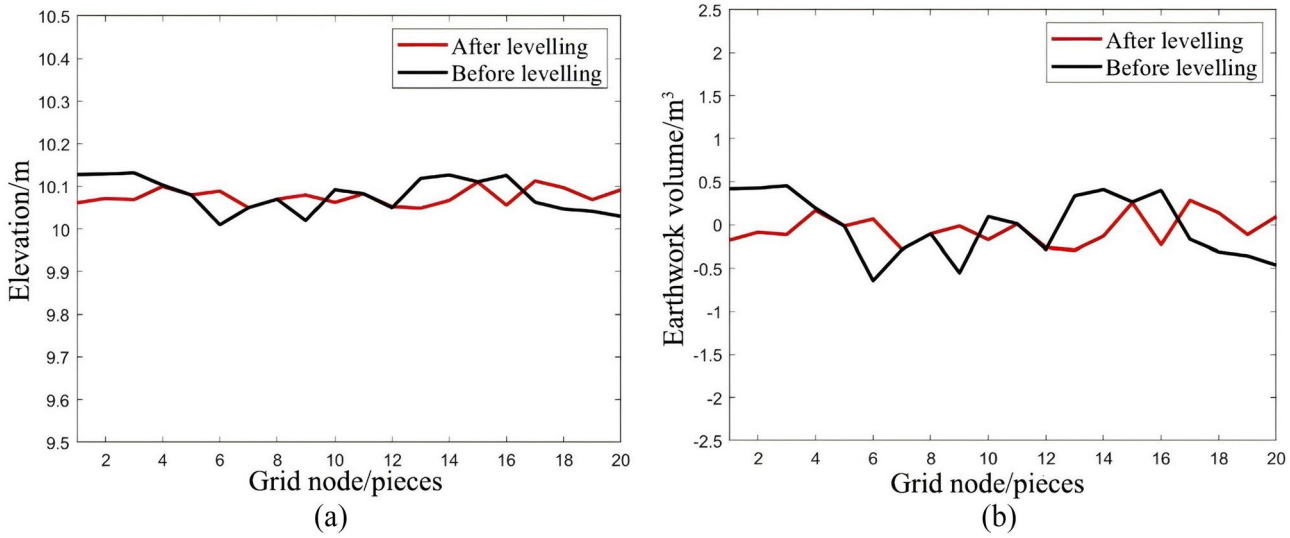

Fig. 21. Elevation and earthwork volume information of grid nodes along the inter-regional path before and after the operation. (**a**) Elevation of grid nodes along the interregionalpath before and after the operation. (**b**) Earthwork volume of grid nodes along theinter-regional path before and after the operation.

Evaluation indicators	Maximum elevation difference/cm	Distribution of 5 cm elevation difference/%	Flatness/cm
Before levelling	12.2	70	4.17
After levelling	6.4	95	1.93

Table 17. Evaluation indicator values of the inter-regional path before and after levelling.

Validation experiment of refined operation path planning effectiveness

This experiment analyzed the levelling effectiveness of the refined operation path planned using the FIA*ACO algorithm. The visualization platform was used to plan the refined operation path for the test field, with the start coordinates at (1, 21, 0.35) and the end coordinates at (26, 14, −0.56), as shown in Fig. 22.

The evaluation indicator values of the refined path before and after levelling were shown in Table 18. Analysis of the table showed that after the refined levelling operation, the maximum elevation difference of the path decreased by 62.9%, the distribution of the 5 cm elevation difference increased by 52.0%, and the flatness improved by 78.4%. The refined path demonstrated further improvement in levelling effectiveness compared to the inter-regional path.

The elevation information of grid nodes along the refined path before and after the operation was shown in Fig. 23a, and it was converted into earthwork volume information as shown in Fig. 23b. Analysis of the

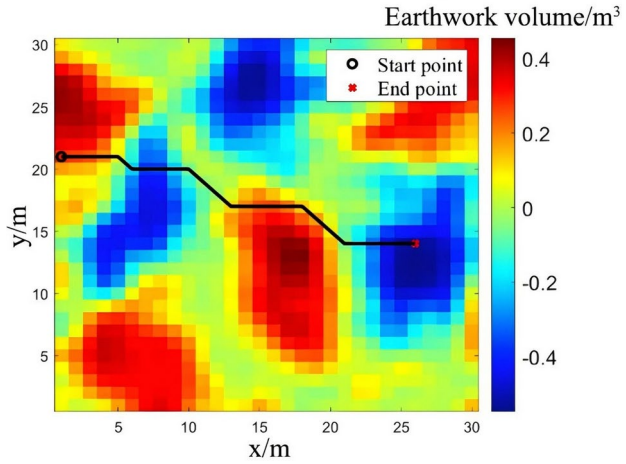

Fig. 22. Refined operation path planning based on the visualization platform.

Evaluation indicators	Maximum elevation difference/cm	Distribution of 5cm elevation difference/%	Flatness/cm
Before levelling	14.0	46.1	5.18
After levelling	5.2	96.1	1.12

Table 18. Evaluation indicator values of the refined path before and after levelling.

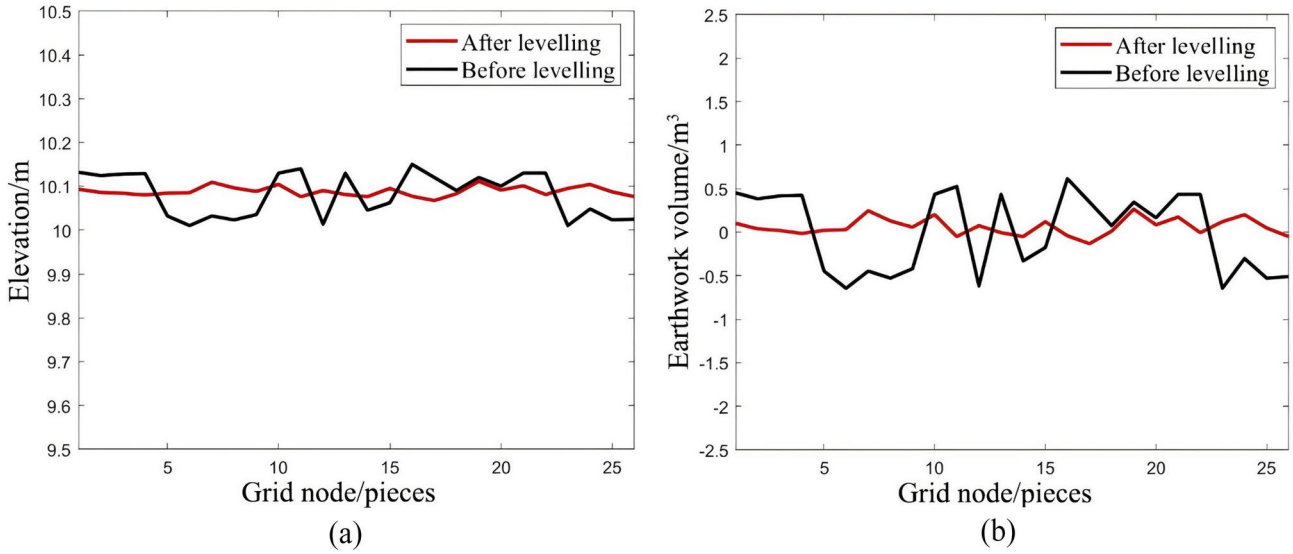

Fig. 23. Elevation and earthwork volume information of grid nodes along the refined path before and after the operation. (**a**) Elevation of grid nodes along the refined path before and after the operation. (**b**) Earthwork volume of grid nodes along the refined path before and after the operation.

figures showed that the ideal earthwork volume for the planned refined operation path was 5.51 m^3, and the actual earthwork volume after levelling was 4.91 m^3. The ratio of actual to ideal earthwork volume was 89.1%, indicating that the refined path achieved better earthwork transfer effectiveness compared to the inter-regional path, meeting the requirements for practical field levelling operations.

Discussion and conclusions

1. To address the issues of large data volumes in land leveling operation path planning, this paper proposed an improved ant colony optimization algorithm for large-scale inter-region earthwork balance operation path planning, and designed an integrated improved A* ant colony optimization algorithm for small-scale,

fine-grained field leveling operation path planning. The IACO was proposed for the path planning of inter-region earthwork balance operations. Initially, the earthwork volume along the operational search paths between high and low terrain regions was incorporated into the heuristic function, which took into account both the inter-region distance and the earthwork to be completed in each region. Subsequently, the weight factor of the heuristic function and the pheromone evaporation factor were adaptively adjusted to enhance the function's effectiveness at different stages of the search path, thereby better aligning with the practical requirements of leveling operations. The FIA*ACO was proposed for the fine-grained leveling operation path planning of the entire field. The first step was to improve the heuristic factor in the evaluation function of the A* algorithm by considering the load of the leveling blade at the parent node. Next, the pheromone update strategy in the ACO algorithm was enhanced with a reward-punishment mechanism to update the pheromone, encouraging ants to explore more optimal paths and reducing the total path length.

2. To evaluate the performance of the IACO-based inter-region earthwork balance operation path planning and the FIA*ACO-based fine-grained leveling operation path planning, simulation tests were conducted on farmlands with varying terrain conditions. The results indicated that, when implementing inter-region path planning in farmlands 1 and 2, the IACO-based leveling operations reduced the empty load rate by 17% and 16.6%, respectively, compared to the ACO. Additionally, the full load rate decreased by 19.1% and 19.65%, respectively; the total path length was reduced by 25.1% and 29.9%, respectively; and the proportion of empty load travel diminished by 53.46% and 36.55%, respectively. In the context of grid-based path planning for farmlands 1 and 2, the FIA*ACO-based leveling operations led to a reduction in the combined empty and full load rate by 15.9% and 10.66%, respectively; the total path length was decreased by 29% and 27.9%, respectively; the total number of paths was reduced by 28.2% and 32.6%, respectively; and the remaining earthwork in the fields post-operation accounted for 47.06% and 35% of the ACO results. These findings confirmed that the proposed improved ant colony optimization algorithm offered enhanced leveling performance, increased operational efficiency, and broader applicability across diverse terrains.
3. To verify the effectiveness of the land leveling path planning based on the variable-scale step-by-step strategy designed in this study, field experiments were conducted on a test field. The results showed that, following the inter-region operation path planning, the maximum elevation difference of the path decreased by 47.5%, the distribution of the 5 cm elevation difference increased by 26.3%, and the flatness improved by 53.7%. Subsequently, after the inter-grid operation path planning, the maximum elevation difference of the path decreased by 62.9%, the distribution of the 5 cm elevation difference increased by 52.0%, and the flatness improved by 78.4%. The inter-region operation path planning rapidly increased the area of the field meeting the leveling requirements, while the subsequent inter-grid operation path planning was used for full-field fine search planning, further increasing the area meeting the flatness requirements. This confirmed the effectiveness of the variable-scale stepwise planning strategy for leveling operation path planning as proposed in this study. Currently, the improved ant colony algorithm provided optimal solutions mainly for rectangular plots but encountered limitations when applied to smaller or more fragmented land areas. In future work, we intend to evaluate the method's performance through further optimizing the parameters of the algorithm and further refine it to address the challenge of path optimization for autonomous land levelling in polygonal fields under unmanned farm operations.

Data availability

All data generated or analysed during this study are included in this published article.

Received: 15 December 2024; Accepted: 11 March 2025
Published online: 21 March 2025

References

1. Li, F., Xu, D. & Li, Y. Effectiveness evaluation and combined application of land leveling technologies. *Nongye Gongcheng Xuebao (Trans. Chin. Soc. Agric. Eng.)* **16**(2), 50–53 (2000).
2. Chen, G. et al. A review of global precision land-leveling technologies and implements: Current status, challenges and future trends. *Comput. Electron. Agric.* **220**, 108901 (2024).
3. Bueno, M. V. et al. Demarcation of levees in irrigated rice fields: Laser technology vs. GNSS-RTK. *Appl. Eng. Agric.* **35**(3), 431–437 (2019).
4. Sidhu, H. S., Singh, S. K. & Pandey, H. S. Performance evaluation of automatic vis-à-vis manual topographic survey for precision land levelling. *Precis. Agric.* **21**, 300–310 (2020).
5. Gagnon, P., Chrétien, F. & Thériault, G. Land leveling impact on surface runoff and soil losses: Estimation with coupled deterministic/stochastic models for a Québec agricultural field. *J. Hydrol.* **544**, 488–499 (2017).
6. Enciso, J. et al. Assessing land leveling needs and performance with unmanned aerial system. *J. Appl. Remote Sens.* **12**(1), 016001–016001 (2018).
7. Nilsson, R. S. & Zhou, K. Method and bench-marking framework for coverage path planning in arable farming. *Biosyst. Eng.* **198**, 248–265 (2020).
8. Kang, X., Li, X. & Xia, Y. Design of fast land leveling system based on GNSS. *Trans. Chin. Soc. Agric. Mach.* **47**(S1), 13–20 (2016).
9. Xia, Y., Liu, G. & Kang, X. Optimization and analysis of location accuracy based on GNSS-controlled precise land leveling system. *Trans. Chin. Soc. Agric. Mach.* **48**(S1), 40–44 (2017).
10. Li, X., Li, H., Niu, D., Wang, Y. & Liu, G. Optimization of GNSS-controlled land leveling system and related experiments. *Trans. Chin. Soc. Agric. Eng.* **31**(3), 48–55 (2015).
11. Jing, Y., Kang, X., Xia, Y., & Liu, G. Automatic steering system for land leveling based on GNSS. In *2018 ASABE Annual International Meeting* (p. 1). American Society of Agricultural and Biological Engineers (2018).
12. Jing, Y., Liu, G. & Luo, C. Path tracking control with slip compensation of a global navigation satellite system based tractor-scraper land levelling system. *Biosyst. Eng.* **212**, 360–377 (2021).
13. Gang, L., Xiao, L., Xi, K., Youxiang, X., & Dongling, N. Automatic navigation path planning method for land leveling based on GNSS. *Nongye Jixie Xuebao/Trans. Chin. Soc. Agric. Mach.* (2016).

14. Liu, G., Kang, X., Xia, Y. X. & Jing, Y. P. Global path planning algorithm and experiment based on GNSS-controlled precise land leveling system. *Trans. CSAM* **49**(5), 27–33 (2018).
15. Jing, Y., Jin, Z. & Liu, G. Three dimensional path planning method for navigation of farmland leveling based on improved ant colony algorithm. *Trans. Chin. Soc. Agric. Mach* **51**, 333–339 (2020).
16. Ojima, I., & Date, H. Path planning for a land leveler. In *2019 IEEE/SICE International Symposium on System Integration* (SII), 222–226 (IEEE, 2019).
17. Jeon, C. W. et al. Autonomous paddy field puddling and leveling operations based on full-coverage path generation and tracking. *Precis. Agric.* **25**(1), 235–256 (2024).
18. Jing, Y., Luo, C. & Liu, G. Multiobjective path optimization for autonomous land levelling operations based on an improved MOEA/D-ACO. *Comput. Electron. Agric.* **197**, 106995 (2022).
19. Zhang, L. et al. Estimating leaf chlorophyll content of winter wheat from UAV multispectral images using machine learning algorithms under different species, growth stages, and nitrogen stress conditions. *Agriculture* **14**(7), 1064 (2024).
20. Luo, Q., Wang, H., Zheng, Y. & He, J. Research on path planning of mobile robot based on improved ant colony algorithm. *Neural Comput. Appl.* **32**, 1555–1566 (2020).
21. Liu, J., Yang, J., Liu, H., Tian, X. & Gao, M. An improved ant colony algorithm for robot path planning. *Soft Comput.* **21**, 5829–5839 (2017).
22. Deng, W., Xu, J. & Zhao, H. An improved ant colony optimization algorithm based on hybrid strategies for scheduling problem. *IEEE Access* **7**, 20281–20292 (2019).
23. Gao, Y. et al. Optimization of operating parameters for straw returning machine based on vibration characteristic analysis. *Agronomy* **14**(10), 2388 (2024).
24. Zhang, L. et al. Estimating winter wheat plant nitrogen content by combining spectral and texture features based on a low-cost UAV RGB system throughout the growing season. *Agriculture* **14**(3), 456 (2024).
25. Niu, Y. et al. Enhancing model accuracy of UAV-based biomass estimation by evaluating effects of image resolution and texture feature extraction strategy. *IEEE J. Select. Top. Appl. Earth Observ. Remote Sens.* **18**, 1–15 (2024).

Acknowledgements

This work was supported by Jiangsu Provincial Agricultural Science and Technology Independent Innovation Project (Grant number CX(22)2040). Laboratory was provided by Key Laboratory for Theory and Technology of Intelligent Agricultural Machinery and Equipment of Jiangsu University, Zhenjiang, China. Thanks to Professors Xinhua Wei and Chengliang Liu for their guidance. Thanks to Jiaxin Yang, Lei Sun, Shaocen Zhang, Anzhe Wang, Xinying Zhou, Fei Wang et al. for their experimental program discussion and experimental assistance.

Author contributions

Conceptualization, Xinhua Wei and Chengliang Liu; methodology, Jiaxin Yang; software, Wenming Chen; validation, Wenming Chen; formal analysis, Wenming Chen; investigation, Shaocen Zhang and Anzhe Wang; resources, Xinying Zhou and Lei Sun; data curation, Wenming Chen; writing—original draft preparation, Wenming Chen; writing—review and editing, Fei Wang; visualization, Xinhua Wei; supervision, Xinhua Wei; project administration, Xinhua Wei; funding acquisition, Xinhua Wei. All authors have read and agreed to the published version of the manuscript. All authors reviewed the manuscript.

Funding

This study was funded by Jiangsu Provincial Agricultural Science and Technology Independent Innovation Project (Grant number CX(22)2040).

Declarations

Competing interests

The authors declare no competing interests.

Additional information

Correspondence and requests for materials should be addressed to X.W.